CHAPTER 4

CHAPTER 4

Synthesis, Characterization, Interfacial and Dispersion Behaviour of Amino Acid Base Metallosurfactants

ABSTRACT

Dicarboxylic amino acid based metallosurfactants were synthesized by stoichiometric mixing of [(C_{12}AAS)Na_2] with bivalent metal salts $CaCl_2$, $MnCl_2$ and $CdCl_2$. Water insoluble coacervates formed were isolated by solvent extraction technique using chloroform. Metallosurfactants formed layered structure as described by X-ray diffraction studies. Thermal phase transition and weight loss of the synthesized compounds were investigated by thermo gravimetric analysis. Monomolecular films of the metallosurfactants in combination with soy phosphatidylcholine (SPC) were investigated using a Langmuir surface balance with intention to substitute naturally occurring phospholipids. With increasing mole fraction of metallosurfactants [$\alpha_{(C_{12}AAS)_2M_2}$], mean molecular area values gradually increased, indicating reorganization of molecular packing at air-water interface, whereby collapse pressure did not change significantly. In case of 20 and 60 mole% (C_{12}AAS)$_2M_2$, positive deviations were recorded indicative of chain mis-match among the components of mixed monolayer. Synergistic interactions between the components at the air-water interface were established from negative deviation of the experimental parameters with reference to the theoretically predicted values. Dynamic surface elasticity, examined by surface rheology studies, initially increased rapidly in the surface pressure range 0 to 1.5 mN/m, after which the slope of surface elasticity *vs.* surface pressure profiles decreased indicating formation of relatively rigid monolayers. Brewster angle microscopic (BAM) studies suggested two dimensional phase transition from gaseous to liquid expanded to liquid condensed state of the monolayers upon compression. BAM images demonstrated homogeneous and more condensed structure of surface layer and confirmed miscibility of the components. Metallosurfactants in combination with SPC and cholesterol could form stable hybrid vesicles. Hydrodynamic diameter, zeta potential and polydispersity index values were measured by dynamic light scattering studies. DSC studies were monitored as function

of time to check the stability of hybrid vesicles. Vesicles were found to be stable upto 100 days. Size, surface morphology and bilayer thickness were investigated by transmission electron microscopic studies that were comparable with the dynamic light scattering studies. Thermodynamic parameters associated with the chain melting processes of the bilayer were investigated by differential scanning calorimetric studies. Cytotoxicity of the vesicles were assessed by MTT and cell viability studies. Such systems are considered to have possible applications as drug carrier involving sustained and controlled release.

1. INTRODUCTION

Functionalizations of complex metal atoms with surfactants have become interesting in research area due to their stable linkage. The effective functionalities develop a potential class of material termed metallosurfactant. Metallosurfactants are capable to form micelle, vesicle, liquid crystal and bilayer that depend on different environmental condition like temperature, salinity, pressure and solvent nature, *etc*.[276-278] Anionic amino acid based surfactant (C_{12}AAS)Na_2 interacts with bivalent (Ca^{2+}, Mn^{2+} and Cd^{2+}) counterion to form water insoluble metallosurfactants. (C_{12}AAS)Na_2 having two alkyl chains that considered as a pseudo double-tailed amphiphiles. Two alkyl chains are connected together due to the strong electrostatic interactions between the two bivalent metal ions and two dicarboxylic amino acids; these complexes have very low solubility in water. Counterions (herein the bivalent metal ions) to the (C_{12}AAS)Na_2 that eventually form the metallosurfactant, play crucial rules in forming the bilayer structure where the hydrophobic part remain delineated from water, a necessary condition for the formation of unilamellar vesicle.[28, 29]

Physicochemical properties of liposome largely depend on head group charge, chain length of the hydrocarbon moiety, intra/inter molecular interaction and environmental conditions.[279, 280] Stability of the vesicles are controlled by different factors, *viz.* amphiphile composition, surface charge and hydrodynamic size.[281] These neoteric phospholipids mimic amphiphile spontaneously formed stable vesicles. Hydrophobic component of the metallosurfactants can interact with lipid acyl chain of SPC to

form stable vesicles.[282-284] Cholesterol is the key components of bilayer which regulates the fluidity and rigidity of the membrane.[285] In the present study, 30 mole% cholesterol with respect to the total amphiphile was used.

Physicochemical properties of biological cells membranes are governed by the compositions, which subsequently regulate its different mode of action.[286,287,288] Potential activity of the biological cell membrane are regulated using phospholipids, cholesterol and regulatory protein. Phospholipids are major components of biological cell membrane because they are able to exhibit the amphiphile nature. Drug carrying capability arises due to its hydrophilic and hydrophobic nature, whereby vesicle is the subject for their biocompatibility and stability. Liposomes find versatile applications for its ease of preparation, resemblance to model membrane systems, biocompatibility, and stability, *etc*.[289, 290]

Metallosurfactants derived from transition metals have been functional materials in biological area and material science.[291] The origin of such materials with cadmium based metallosurfactant has been interested in solid state and catalytic chemistry as well as manganese containing metallosurfactant has been used potent sensitizing agents capable of inducing hypersensitivity due to the structural stabilities.[292,293] Damaged kidneys are incapable of proper calcium absorption into the bodily systems, which is essential for the maintenance of bones.[293] Calcium, manganese and cadmium based metallosurfactants can exhibit chelating properties, bind to harmful metals that can be removed through excretion. Cadmium gets accumulated in kidney, liver and other organs by binding to metallothioneis which eventually results in cell toxicity.[294] Studies on the remedial measures involving long term exposure to heavy metals are not abundant in literature. Toxicity remains unrecognized in its early stage as the chelation therapy is not very effective for Cd^{2+} and Mn^{2+}. As these bivalent metals can electrostatically bind to $C_{12}AAS^{2-}$ ions, hence the complexes are expected to be insoluble in water. Consequently the metallosurfactants are expected to form vesicles in combination with naturally occurring phospholipids. Such hybrid vesicles, therefore, can remove or supplement the aforementioned

bivalent metals, as and when required. Thus proper understandings on the physicochemistry of metallosurfactants are considered worthy of investigation.

Physicochemistry of metallosurfactants shows many fold applications such as recovery of complexes,[28] ultra-filtration,[29] removal of organic pollutants,[144] enhanced recovery of oil,[145] removal of heavy metal from waste water,[146] synthesis of mesoporous materials, adsorption, batteries, catalysis, ceramic precursors, nonlinear optics, electronic conductivity and sensors.[147] Naturally occurring phospholipids are widely used for synthesis the vesicle and shows different versatile application, *viz.* drug delivery,[7] gene therapy,[8] DNA transfection[9] and nano particle synthesis.[9, 10]

Present work describes the synthesis, characterization, interfacial and bilayer (in the form of hybrid vesicles) behaviors of metallosurfactants in combination with naturally occurring phospholipid, soyphosphatidylcholine and cholesterol. Metallosurfactants were characterized by NMR, FTIR and X-ray diffraction studies. Thermotropic behavior and associated thermodynamic parameters were also evaluated by analyzing the DSC data. These include melting temperature of the bilayer (T_m), full width at half maximum of T_m ($\Delta T_{1/2}$), change in enthalpy (ΔH) and molar heat capacities (ΔC_p) of metallosurfactants. Solvent spread monomolecular films of metallosurfactant + SPC mixtures in combination with 30 mole% cholesterol were raveled by a Langmuir balance at air-water interface. Surface rheologies of mixed monolayer systems were also investigated. Moreover the hydrodynamic size and zeta potential values of the vesicles studied at different combinations as well as time in order to check their stabilities by way of DLS studies. Morphology and bilayer thickness were established by TEM measurements. Cytotoxicity studies of the vesicles towards human peripheral lymphocytes were carried out in order to explore their therapeutic applications.

Till date no comprehensive studies on metallosurfactants are available in literature. Studies on the interfacial and morphologies behavior of metallosurfactant+SPC mixture being provide metal deficiencies in human body. Metallosurfactants, in combination with natural phospholipids in the form of vesicles, are considered for drug encapsulation, antibacterial formulation and nanomaterial synthesis.[193] Also, such

systems are expected input the drug into vesicles would have studied the release kinetics and entrapment efficiency being considered as the future perspectives.

2. EXPERIMENTAL SECTION

2.1. ***Materials.*** Commercially available soy phosphatidylcholine was a product of EMD Chemicals, Germany. $CaCl_2$. $4H_2O$, $MnCl_2$. $2H_2O$, $CdCl_2$. $5H_2O$ (A. R. grade) and chloroform (HPLC grade) were the products from Merck specialties Pvt. Ltd. India. Dodecyl chloride, *L*-malonic, aspartic and glutamic acid were purchased from Sigma-Aldrich Chemicals Pvt. Ltd. (USA). Double distilled water with specific conductance of 2-4 μS at 298 K was used in preparing different solutions as well as the subphase for the monolayer studies.

2.2. Methods.

2.2.1. Preparation and isolation of the bivalent metal complex. Stoichiometric amount of aqueous *N*- dodecyl amino -malonate, -aspartate and -glutamate (100 mM dm^{-3}) were separately added drop wise to aqueous $CaCl_2$. $4H_2O$, $MnCl_2$. $2H_2O$ and $CdCl_2$. $4H_2O$ (100 mM dm^{-3}) solution with constant stirring, that resulted in the formation of white colour precipitates. Insoluble components were extracted using chloroform. Synthesized metallosurfactants were finally dried and stored under vacuum.

2.2.2. Crystal XRD studies. X-ray diffractograms of metallosurfactants were obtained by an X-ray diffractometer (Ultima, III, Rigaku, Japan, Cu (K_β) line, with an operating voltage of 40kV and a current of 30mA). Scan speed was set at 1° min^{-1} where the sampling width was set at 0.02°.

2.2.3. ^{1}***H NMR spectroscopy studies.*** ^{1}H NMR spectra of metallosurfactants and its precursors in $CDCl_3$ were recorded in a 500 MHz NMR spectrometer (Bruker, AC, Switzerland). Tetramethylsilane (TMS) was used as the internal standard.

2.2.4. Furrier transformation infrared spectroscopy (FTIR) studies. FTIR studies of the metallosurfactants were recorded by FTIR spectrophotometer (Lambda, 25 Perkin Elmer spectrophotometer, USA) in the range 1250 - 3500 cm^{-1}. Dry Sample was used for FTIR studies.

2.2.5. Differential scanning calorimetry (DSC) studies. Chain melting temperature (T_m) and different thermodynamic parameter of metallosurfactants were determined by DSC studies which ultimately controls the physical state of metallosurfactants. DSC studies were performed using with a differential scanning calorimeter (Pyris 6 DSC-8000, Perkin Elmer, USA). Calibration was made using indium as the internal standard. Metallosurfactants were scanned at 5°C min^{-1} and heating rate was set from 0-273 °C.

2.2.6. Thermogravimetric analysis (TGA) studies. Weight loss and thermal stability of the metallosurfactants were evaluated by TGA. TGA of metallosurfactants were done by Pyris 6 TGA-DTA-8000 (Perkin Elmer, USA). Sample was scan at 20 °C min^{-1}.

2.2.7. Surface pressure (π) - area (A) isotherm. Surface pressure (π) - area (A) isotherm of solvent spread monolayer were studied by Langmuir balance (μ Trough, Kibron, Finland) with a resolution 0.01 mN m^{-1}. The trough and the barriers were comprised of teflon.[123] Trough was filled with the 30 mL water as the sub phase. Metallosurfactants, in combination with stoichiometric amount of soy phosphatidylcholine and cholesterol were dissolved in choloform : methanol (3:1, V/V) and were spread on to the air-water interface using a Hamilton microsyringe (USA). A 20 min equilibration time was allowed for solvent evaporation and equilibration of the monomolecular film.[295]

2.2.8. Surface dilatational studies. Dilatational elasticity modulus (E) of mixed monolayer was evaluated at different surface pressure and calculated from the following equation:[152]

$$E = - \frac{d\pi}{d\ (ln\ A)} \quad (1)$$

where E is the compression modulus. Dilatational modulus values were evaluated using ISR instrument (KSV NIMA, Finland). Monomolecular films are elastic and lowest frequency of deformation which indicate that modulus are frequency independent.[296]

2.2.9. Brewster angle microscopy (BAM) studies. BAM images were recorded with a BAM 2 Plus (NFT, Gottingen, Germany). A 30 mW laser beam emitting p-polarized light at 532 nm was used with the Brewster angle of 53.1°.

2.2.10. Preparation of vesicles. Metallosurfactants were combined with SPC (at 20, 40, 50, 60 and 80 mole %) along with 30 mole% cholesterol to prepare small unilamellar vesicles by thin film generation and rehydration technique.[297-299] Requisite quantities of metallosurfactants, SPC and cholesterol were dissolved in chloroform in a 50 mL round bottom flask. Solvent was evaporated by rotary evaporator whereby a thin film was formed in presence of a stream of nitrogen gas. The obtained thin film was rehydrated with water at an elevated temperature (343K).[154] The dispersion was then exposed to sonication, followed by freezing at sub-zero temperature. The process of freeze-thaw-sonication was repeated three cycles in order to obtain small unilamellar vesicles.

2.2.11. Dynamic light scattering (DLS) studies. Hydrodynamic diameter (d_h), zeta potential (*Z.P.*) and polydispersity index (*PDI*) of vesicles were evaluated by DLS studies.[10, 295] DLS studies were performed with a Zetasizer Nano ZS90, ZEN3690, Malvern Instrument Ltd. U.K. spectrophotometer. A He-Ne leaser of 632.8 nm wavelength was used at a scattering angle of 90°. d_h values can be evaluated using the Stokes-Einstein equation:[153]

$$d_h = \frac{kT}{3\pi\eta D} \tag{2}$$

where k, T, η and D values denote Boltzmann constant, temperature, viscosity of the medium and diffusion coefficient. Zeta potential values were measured with a folded capillary cell at 298K.

2.2.12. Transmission electron microscopic (TEM) studies. Dilute vesicle dispersion was placed on carbon coated 300-mesh copper grid.[153] Excess liquid was removed from the edge of the grid and was

then dried for ten minutes. TEM images were recorded with a Hitachi H-600, Japan with an operational voltage of 80kV.

2.2.13. Assessment of cytotoxicity. 5 ml of human blood diluted (1:1) with phosphate buffer saline (PBS). Histopaque- 1077 was added into the human blood solution and centrifuged at 1500 rpm speed for 40 min.[300] Lymphocytes were re-suspended in RPMI media and supplemented with 10% (w/v) fetal bovine serum (FBS) then incubated at 37°C in a 5% (v/v) CO_2 environment in CO_2 incubator.[251] MTT (3-[4,5-dimethylthiazol-2-yl]-2,5-diphenyltetrazolium bromide) assay was used to estimate the cytotoxicity of vesicles.[252] Then 20 µL of MTT solution was added in microtitre plate, having RPMI-suspended lymphocytes. Then the plate was incubated at 37°C for 4 h to metabolize MTT formazan.[253]

3. RESULTS AND DISCUSSION

3.1. Characterization of the [$(C_{12}AAS)_2M_2$] complex.

3.1.1. Crystal XRD studies. Positions of the atoms in the solid crystal and molecular structure of metallosurfactants can be determined by XRD studies. Characteristic XRD pattern of metallosurfactants are shown in Figure 1.

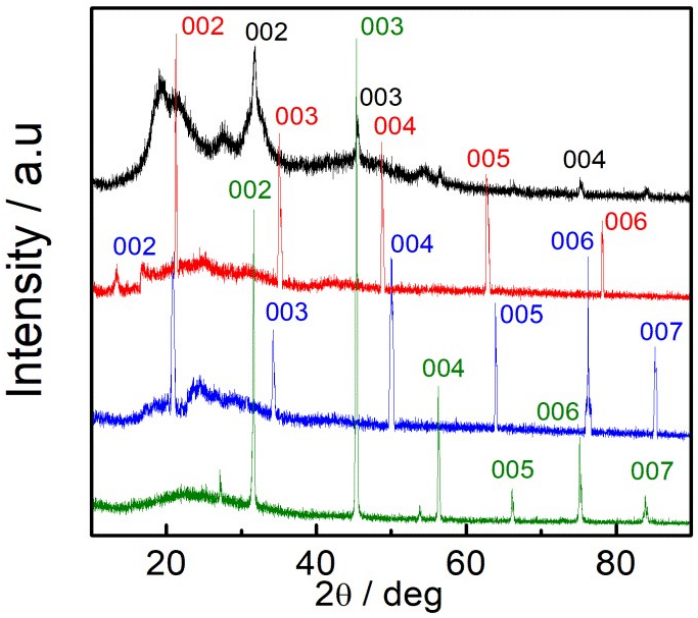

Figure 1. Characteristic XRD spectra of metallosurfactants at 298K. System: A, $C_{12}GluNa_2$; B, $[(C_{12}Glu)_2Cd_2]$; C, $[(C_{12}Glu)_2Ca_2]$; and D, $[(C_{12}Glu)_2Mn_2]$.

Metallosurfactants show different diffraction patterns with at regular interval that correspond to the Miller indices h k 0 or h k *l* having smaller number and weak intensities.[301] The Bragg's angle ($\Delta 2\theta$) between two 0 0 *l* diffraction line were 15.2°, 14.8°, 13.8°, 13.5°, 13°, 12.8°, 12.5°, 12.4° and 12.2° for Cd, Ca and Mn malonate, aspartate and glutamate, respectively. The constant $\Delta 2\theta$ values of metallosurfactants confirmed its lamellar structure. The $\Delta 2\theta$ values are gradually decreased with decreasing the size ($Cd^{2+} > Ca^{2+} > Mn^{2+}$) due to the electrostatic interaction between the two oppositely charged M^{2+} and anionic $(C_{12}AAS)Na_2$. Two carboxylate groups of $C_{12}MalNa_2$, $C_{12}AspNa_2$ and $C_{12}GluNa_2$ are separated by one, two and three methylene groups. Bivalent amino malonate coacervate exhibited higher $\Delta 2\theta$ than aspartate and glutamate due to the hydrophobic interaction between two alkyl chains results packing arrangements of the crystal lattice.[190]

3.1.2. FTIR studies. FTIR spectrums of the metallosurfactants were shown in the Figure 2 - 4.

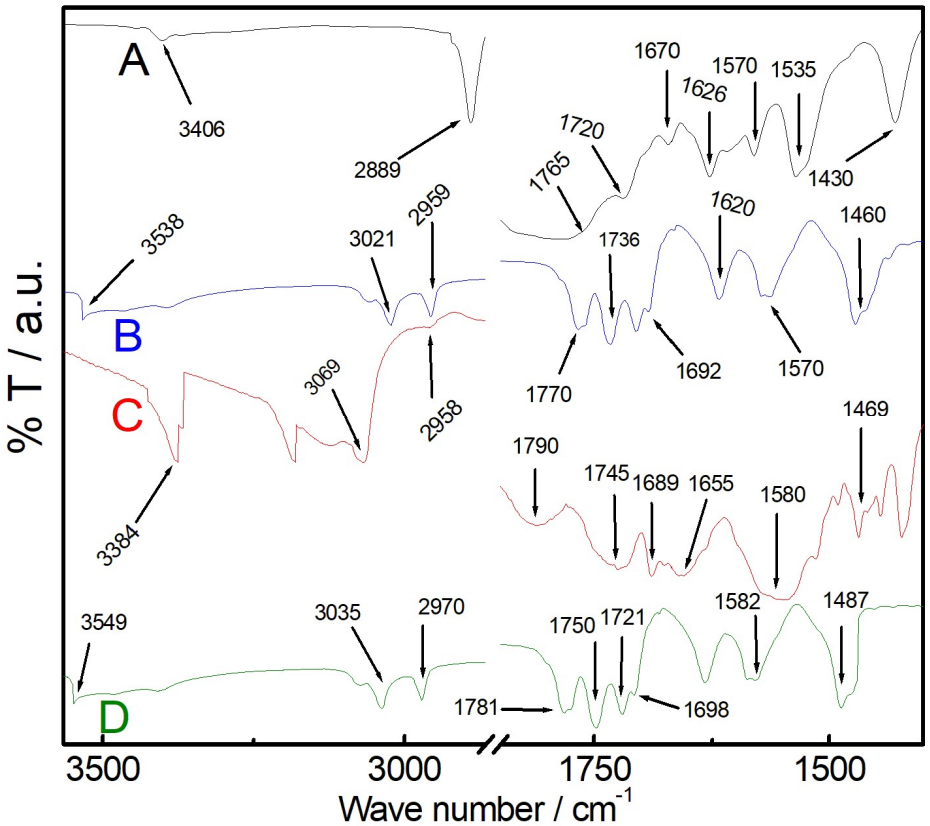

Figure 2. FTIR spectra of aminomalonate-based metallosurfactants at 298K. System: A, $C_{12}MalNa_2$; B, $[(C_{12}Mal)_2Cd_2]$; C, $[(C_{12}Mal)_2Ca_2]$ and D, $[(C_{12}Mal)_2Mn_2]$.

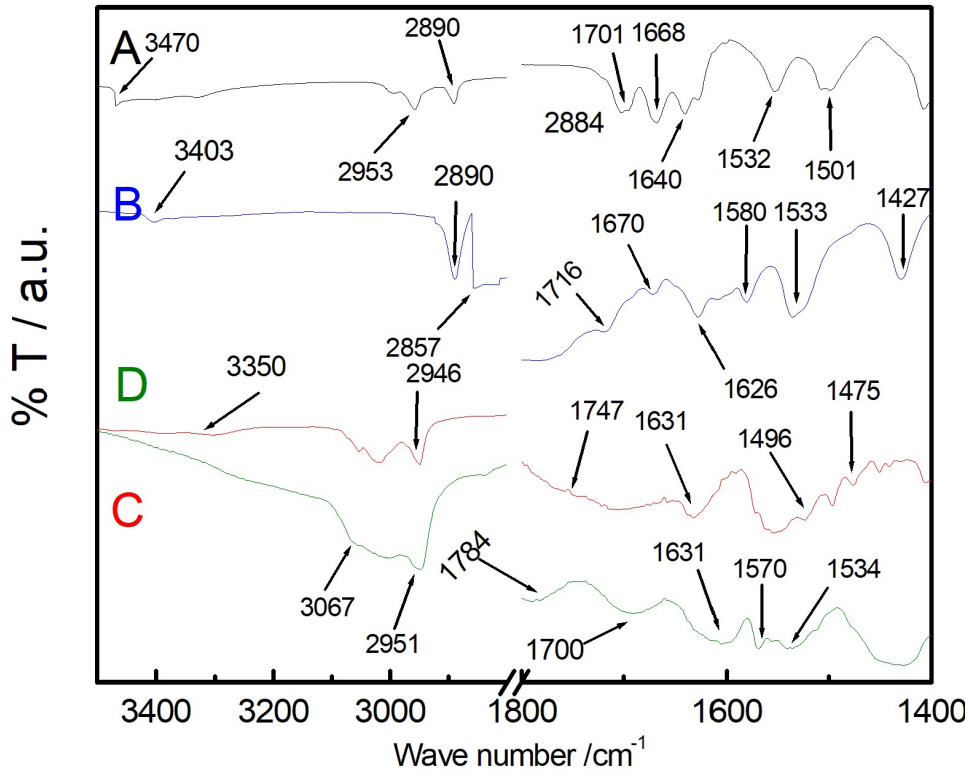

Figure 3. FTIR spectra of aspartate-based metallosurfactantsat 298K. System: A, $C_{12}AspNa_2$; B, $[(C_{12}Asp)_2Cd_2]$; C, $[(C_{12}Asp)_2Ca_2]$ and D, $[(C_{12}Asp)_2Mn_2]$.

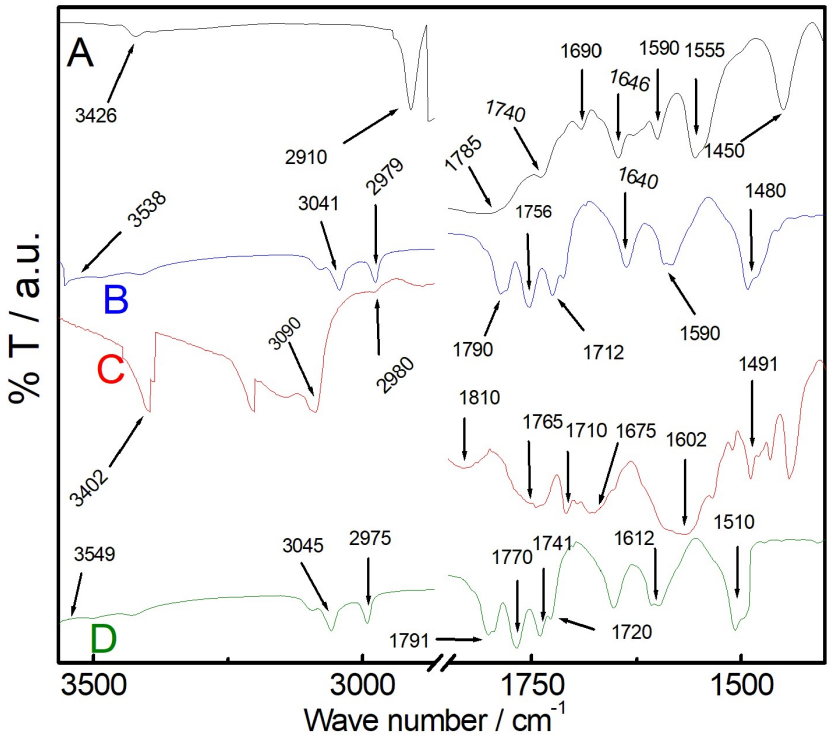

Figure 4. FTIR spectra of glutamate-based metallosurfactantsat 298K. System: A, $C_{12}GluNa_2$; B, $[(C_{12}Glu)_2Cd_2]$; C, $[(C_{12}Glu)_2Ca_2]$ and D, $[(C_{12}Glu)_2Mn_2]$.

The frequency of the complex in the region 3300-3500 cm^{-1} assigned -NH- vibration. The stretching frequency in the region of 2820-2845 and 2890-2930 cm^{-1} displayed asymmetrical and symmetrical

stretching of -CH- bond.[302] Peak at the region 1427-1487 cm^{-1} and 1535-1584 cm^{-1} were assigned asymmetrical and symmetrical stretching of the -CH_2- group because interaction of -$(CH_2)_n$- with electro negative -CO-NH- group, that led to change the charge distribution of α methylene -CH_2- carbon. The -CO-NH- and -CO- group were represented 1630-1690 cm^{-1} and 1680-1750 cm^{-1} stretching frequency in the complex. Bivalent metal ions coordinate with two carboxylate groups of $C_{12}MalNa_2$, $C_{12}AspNa_2$ and $C_{12}GluNa_2$ to form six, seven and eight member cyclic conjugated ring. Smaller size Mn^{2+} electrostatically interacted with carboxylate of $(C_{12}AAS)Na_2$ than Ca^{2+} and Cd^{2+}. Metallosurfactants displayed higher stretching frequencies peak than pure $(C_{12}AAS)Na_2$ due to the higher electrostatic interaction between oppositely charged species. Amino glutamate metallosurfactants exhibited higher frequencies peak because eight member cyclic ring is sterically favourable than seven and six member rings that follows the sequence: manganese glutamate > manganese aspartate > manganese malonate same like Ca and Cd metallosurfactants.

3.1.3. ^{1}H NMR studies. Following ^{1}H NMR results of $(C_{12}AAS)Na_2$ and metallosurfactants are confirmed their structures which was shown Figure 5-16.

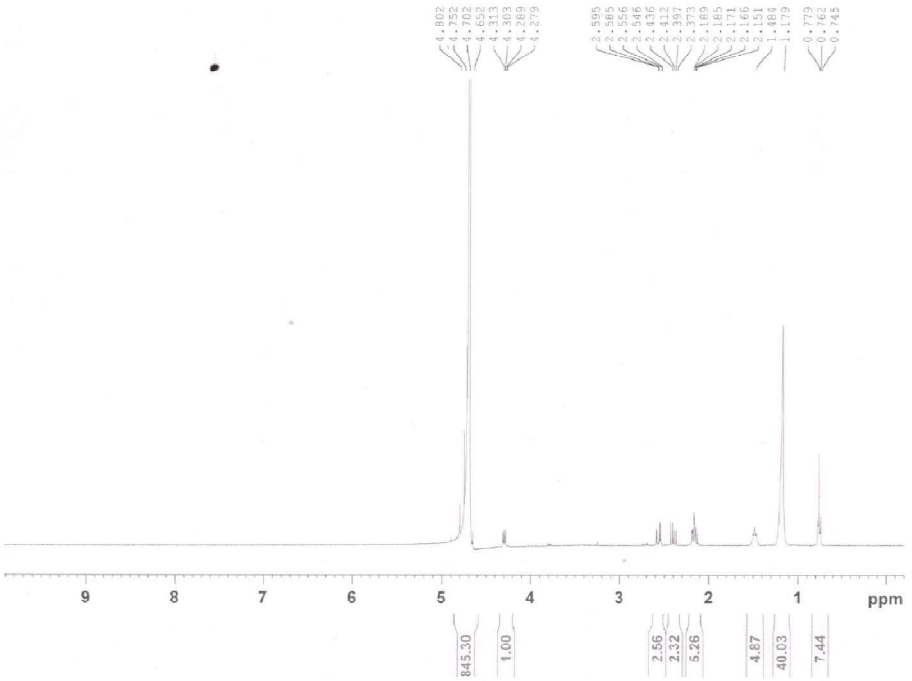

Figure 5. ^{1}H NMR spectrum of sodium aminomalonate ($C_{12}MalNa_2$).

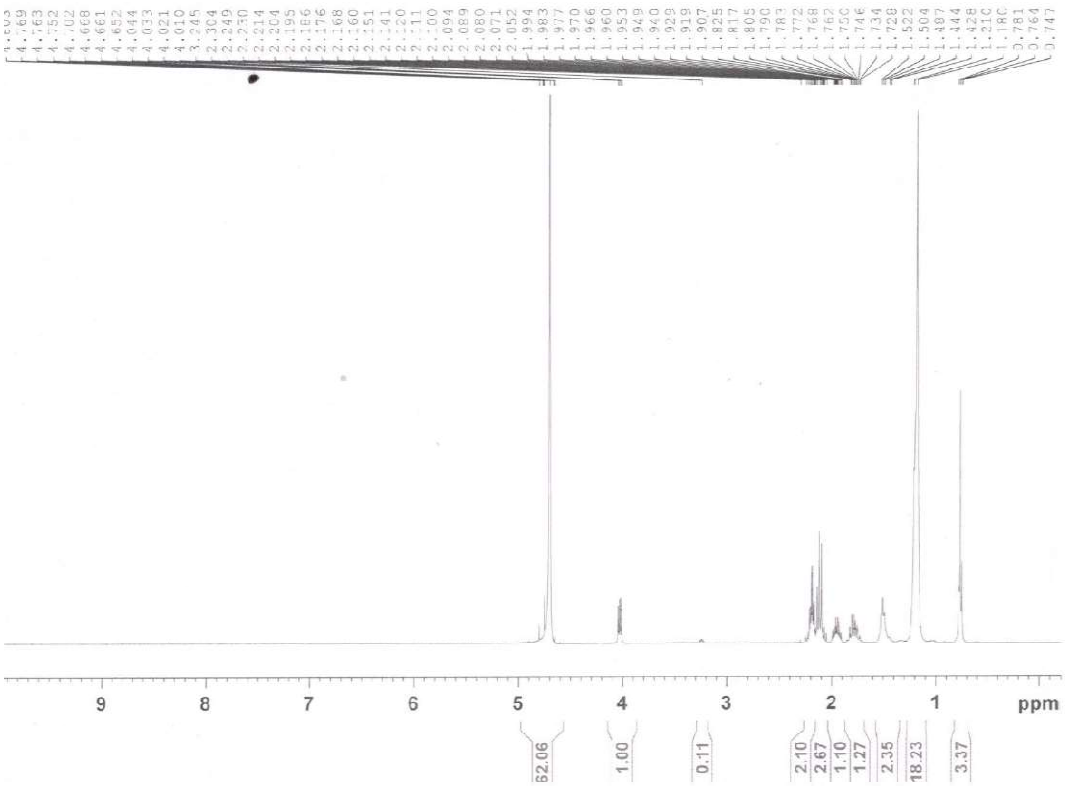

Figure 6. ^{1}H NMR spectrum of sodium aspartate ($C_{12}AspNa_2$).

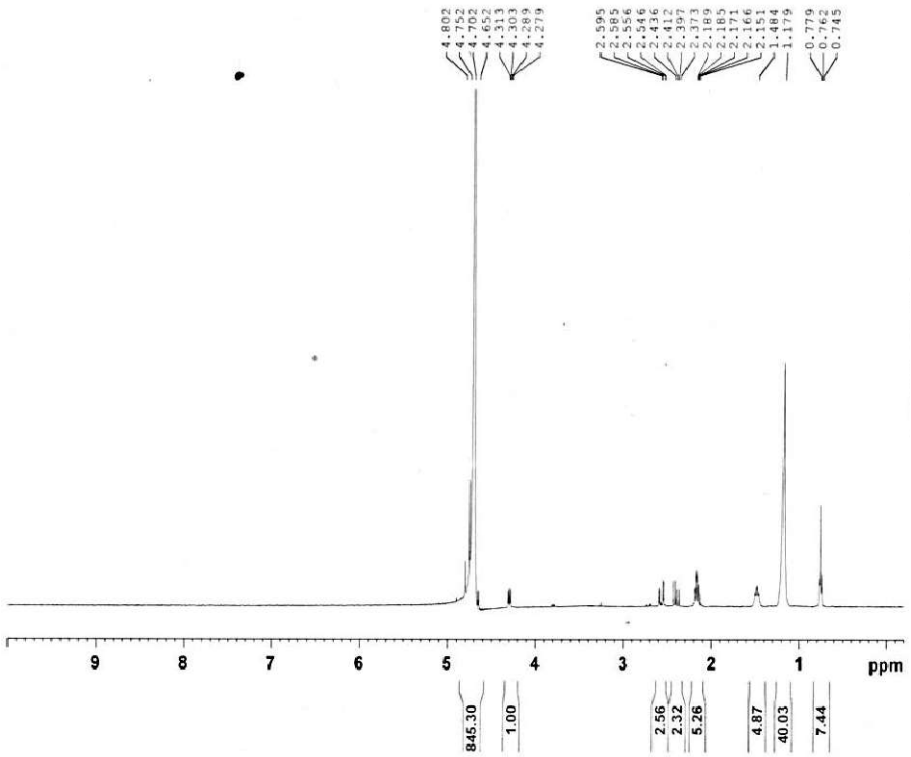

Figure 7. ^{1}H NMR spectrum of sodium glutamate ($C_{12}GluNa_2$).

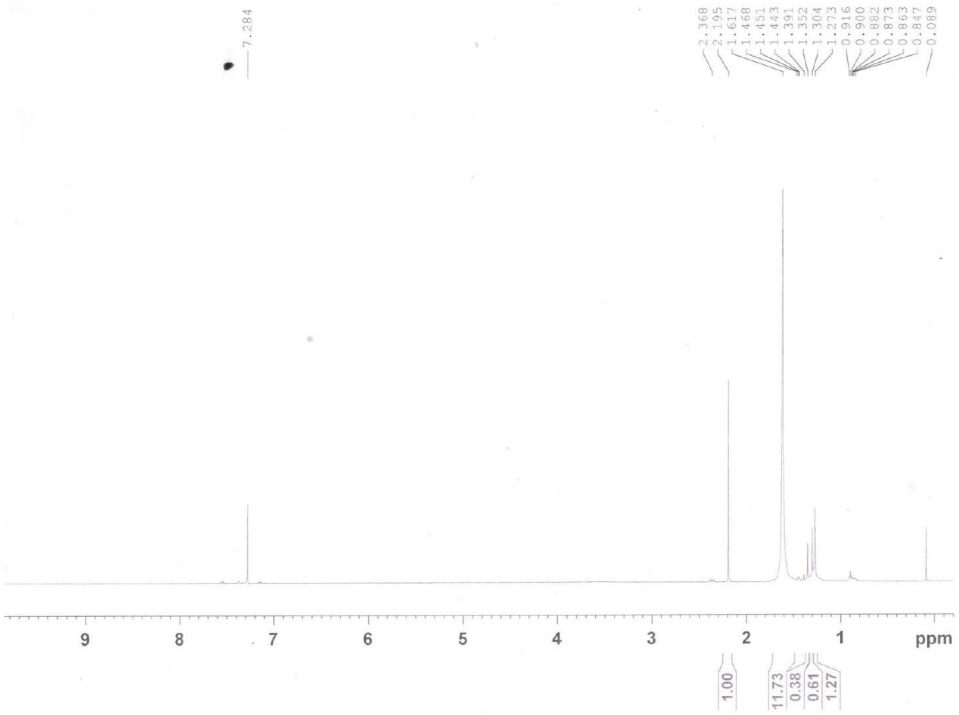

Figure 8. ^{1}H NMR spectrum of calcium aminomalonate [$(C_{12}Mal)_2Ca_2$)].

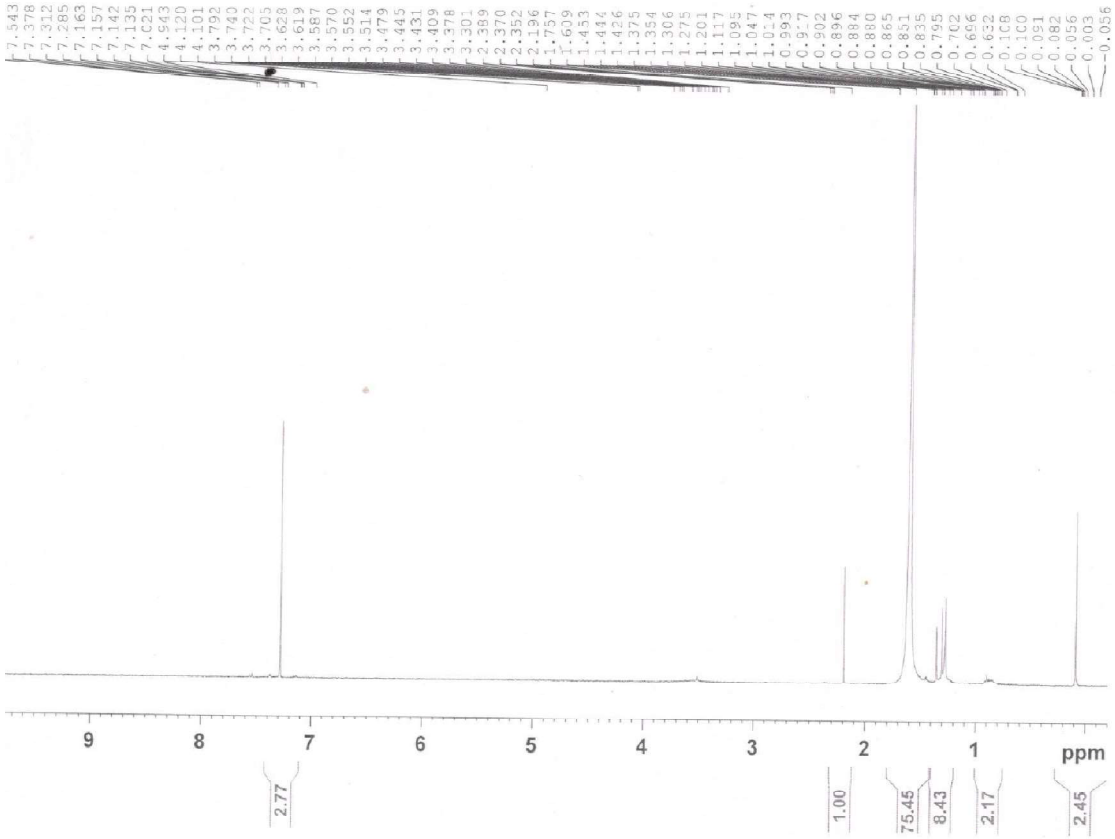

Figure 9. ^{1}H NMR spectrum of calcium aspartate [$(C_{12}Asp)_2Ca_2$]

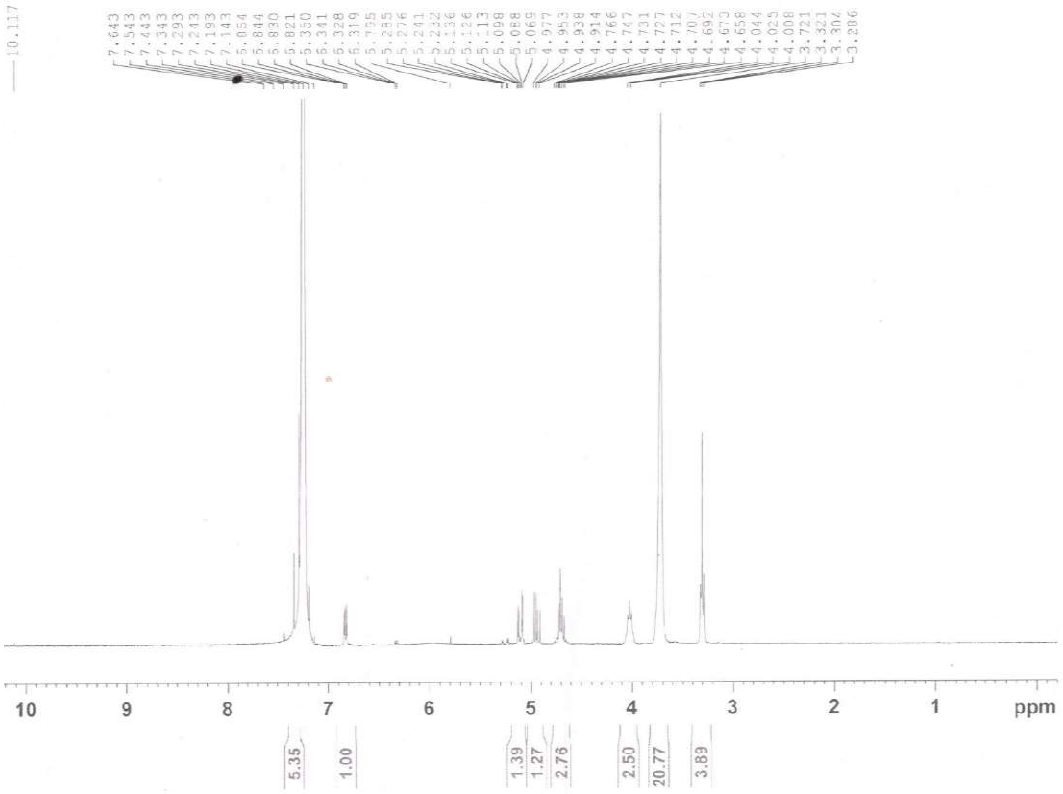

Figure 10. ^{1}H NMR spectrum of calcium glutamate [$(C_{12}Glu)_2Ca_2$].

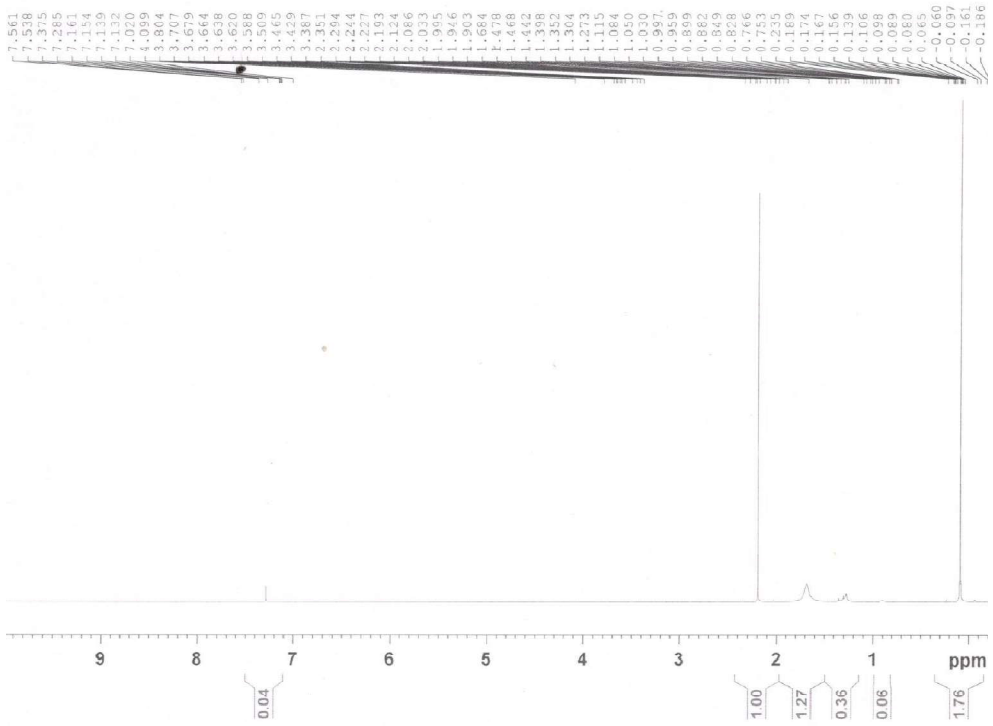

Figure 11. ^{1}H NMR spectrum of manganeseaminomalonate [$(C_{12}Mal)_2Mn_2$].

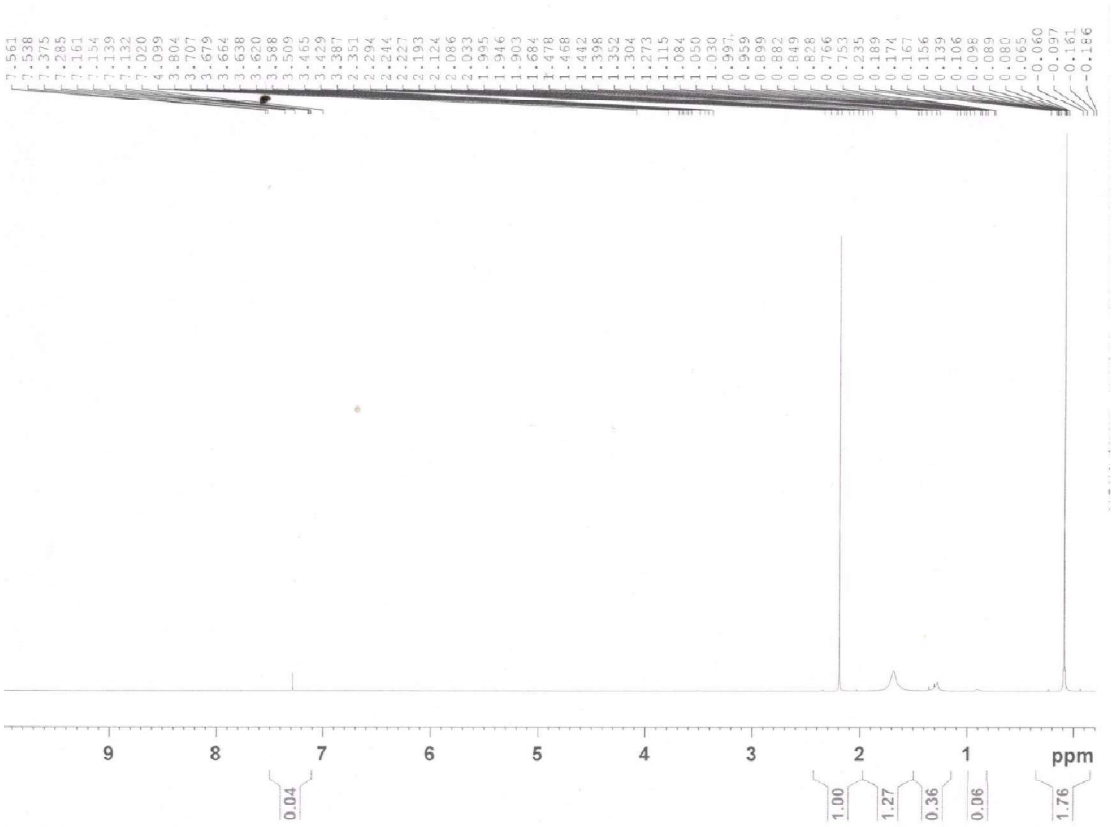

Figure 12. ^{1}H NMR spectrum of manganeseaspartate [$(C_{12}Asp)_2Mn_2$]

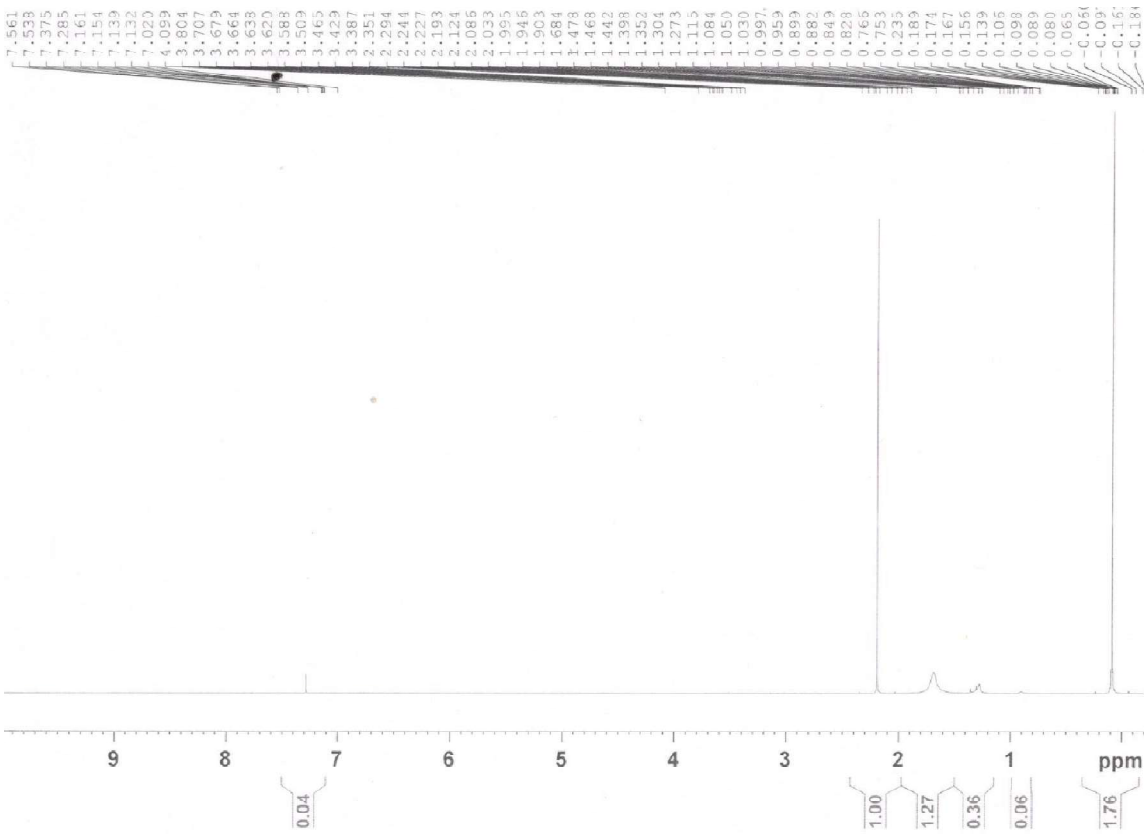

Figure 13. ^{1}H NMR spectrum of manganeseglutamate [$(C_{12}Glu)_2Mn_2$]

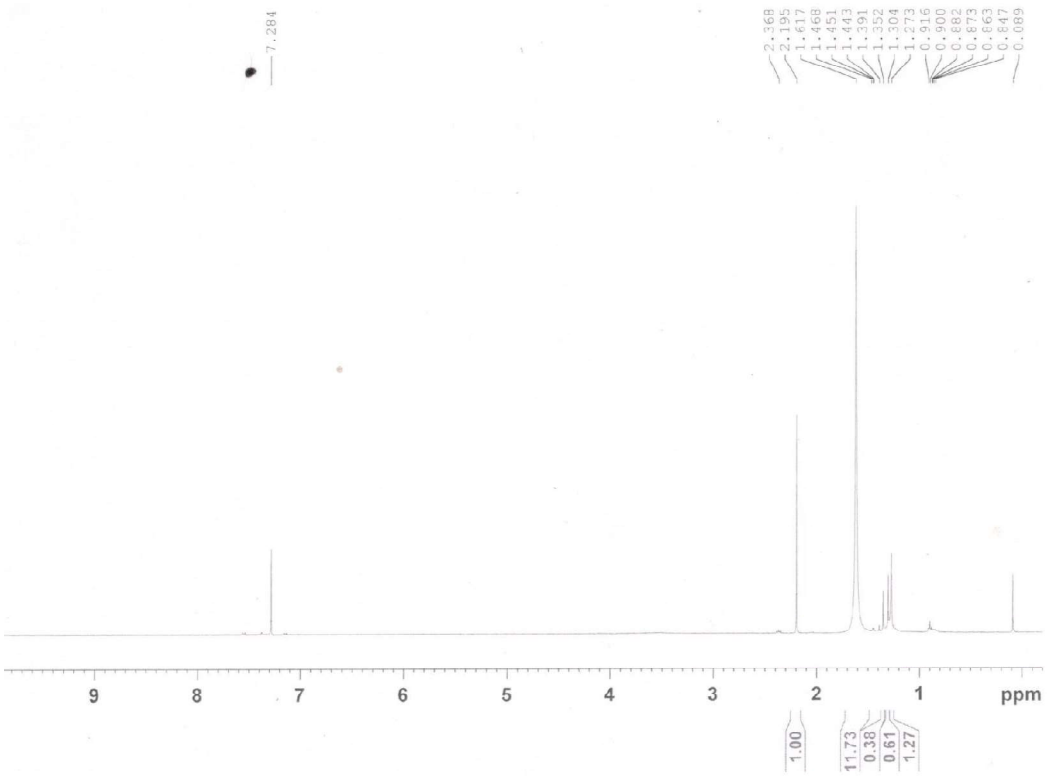

Figure 14. ^{1}H NMR spectrum of cadmiummalonate [$(C_{12}Mal)_2Cd_2$].

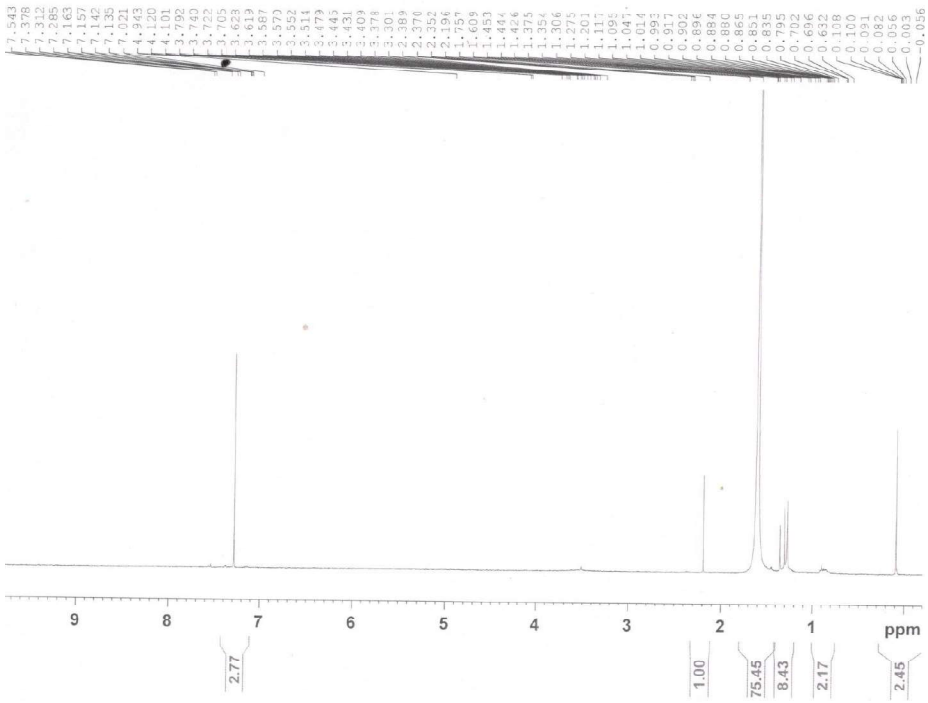

Figure 15. ^{1}H NMR spectrum of cadmium aspartate [$(C_{12}Asp)_2Cd_2$].

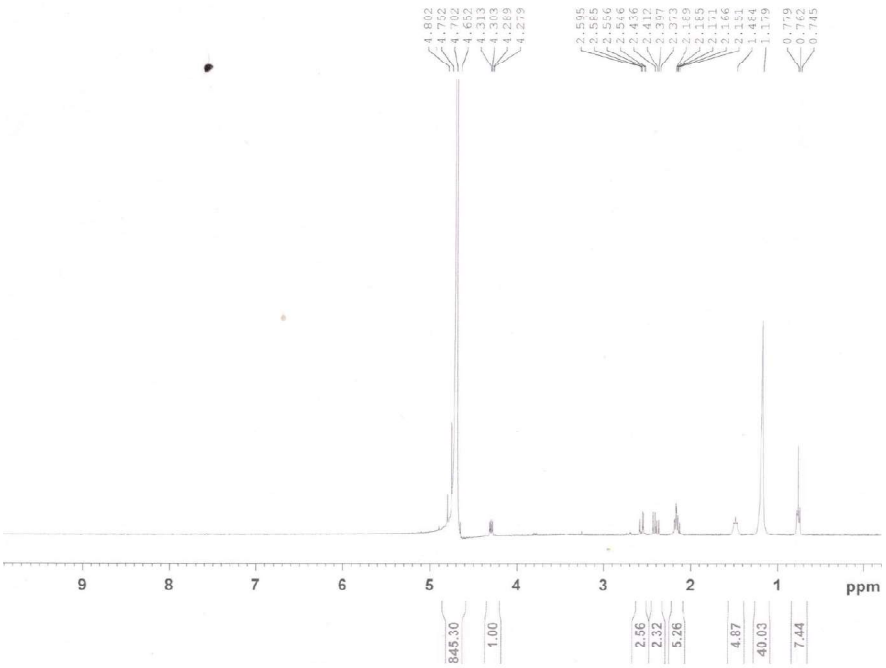

Figure 16. ^{1}H NMR spectrum of cadmium glutamate [$(C_{12}Glu)_2Cd_2$].

$C_{12}GluNa_2$ (500MHz, $CdCl_3$) δ /ppm: 0.86 (t, 3H, ω), 1.23 (s, 14H, $(CH_2)_7$) 1.29 (broad peak, 2H, γ), 1.98 (m, br, 2H, β), 4.94 (m, 2H, α), 4.54 (t, 1H, α, -CO-NH-($^{\alpha}$CH)-), 2.54 (t, 2H, β, -CO-NH-(CH)-$^{\beta}(CH_2)$-), 2.31 (t, 2H, γ, -CO-NH-(CH)-(CH_2)-$^{\gamma}(CH_2)$-) and 5.2 (s, 1H, NH). Similar results were reported by Bordes et al.[124] ^{1}H NMR results of $(C_{12}AAS)Na_2$ helped to identify the different ^{1}H protons of metallosurfactants at different region.

$2C_{12}Glu^{2-}$ M^{2+} (500MHz, $CdCl_3$) δ /ppm: 0.87 (t, 3H, ω, ω), 1.26 (s, 14H, $(CH_2)_7$) 1.36 (broad peak, 2H, γ, γ), 4.25 (m, br, 2H, β), 6.24 (m, 2H, α, α), 4.54 (t, 1H, α', -CO-NH-($^{\alpha}$CH)-), 2.54 (t, 2H, β', -CO-NH-(CH)-$^{\beta}(CH_2)$-), 2.31 (t, 2H, γ', -CO-NH-(CH)-(CH_2)-$^{\gamma}(CH_2)$-) and 5.2 (s, 1H, NH).

^{1}H NMR spectra of metallosurfactants showed characteristics features. The terminal ω, -CH_3 proton of metallosurfactants showed triplet at 0.87 ppm. The single absorption peak at δ = 1.26 ppm correspond to the methylene protons ((-CH_2-)$_7$) after the γ-methylene protons as to be shown in Scheme 1. The NMR peaks of γ -CH_2- protons were in the range of 1.36-1.67 ppm and β -CH_2- protons exhibit the peak at 4.25 ppm. The α-methylene -(-NHCO-$^{\alpha}$CH)- proton with respect to electro negative keto group confirms the

dishelding effect and the corresponding peak appeared in the range 2.54-2.60 ppm. β-methylene -(NHCO-CH-$^{\beta}CH_2$)- proton showed downfield and the peak range of 2.41-2.48 ppm. The γ methylene -NHCO-$CHCH_2{}^{\gamma}(CH_2)$- proton with respect to -NHCO- exhibited up field and the peak at 1.23 ppm for $(C_{12}Glu)_2Mn_2$, $(C_{12}Glu)_2Ca_2$and $(C_{12}Glu)_2Cd_2$. The singlet proton of -NH- displayed downfield and the peak range 5.2-5.8 ppm. ^{1}H NMR values of different proton of metallosurfactants exhibited higher ppm values than pure $(C_{12}AAS)Na_2$ these values gradually increased with decreasing the size of bivalent metal due to the strong electrostatic interaction with anionic carboxylate of $(C_{12}AAS)Na_2$. In consonance with decreasing the size of bivalent metal (M^{2+}) increased the hydrophobic interaction between oppositely charged $(C_{12}AAS)Na_2$ and M^{2+} hence increased the ^{1}H proton NMR peak. Therefore, NMR data was confirmed that formation of the double tailed bivalent metal complex.

3.1.4. Differential scanning calorimetry (DSC) studies. DSC studies were carried out to understand the thermotropic behavior and associated parameters of metallosurfactants. Phase transition temperature and different thermodynamic parameters of metallosurfactants were determined by DSC studies. DSC studies can predict on the nature of physicochemical interaction between bivalent metal (Cd^{2+}, Ca^{2+} and Mn^{2+}) with anionic carboxylate of $(C_{12}AAS)Na_2$. DSC isotherms of metallosurfactants were shown in Figure 17 (panel A).

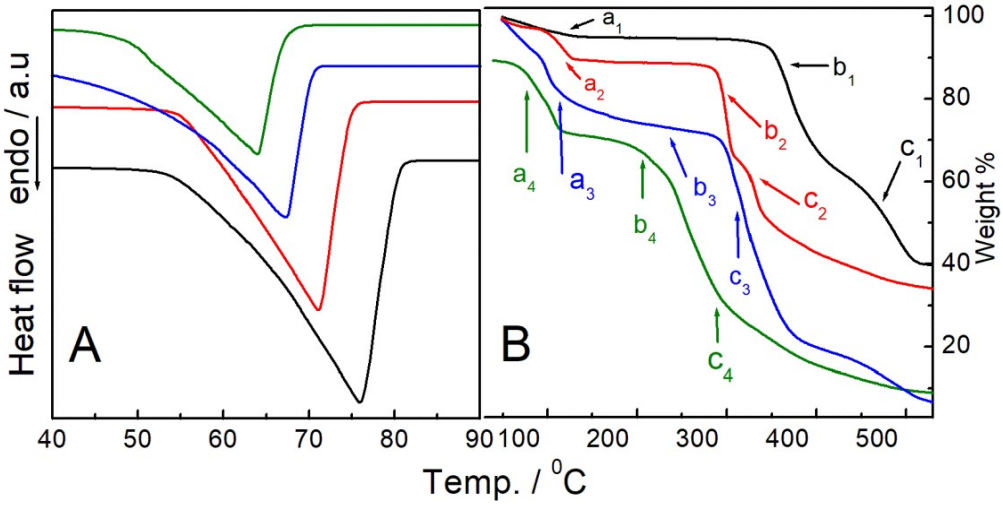

Figure 17. Characteristic (DSC, A) and (TGA, B) profiles of different metallosurfactants. Systems: 1, $C_{12}GluNa_2$; 2, $[(C_{12}Glu)_2Cd_2]$; 3, $[(C_{12}Glu)_2Ca_2]$and 4, $[(C_{12}Glu)_2Mn_2]$.

Metallosurfactants exhibited endothermic peaks in the temperature range 60-85°C, that correspond to the phase transition and hydrocarbon chain melting processes. The T_m, $\Delta T_{1/2}$, ΔH and ΔCp values of the metallosurfactants are shown Figure 18.

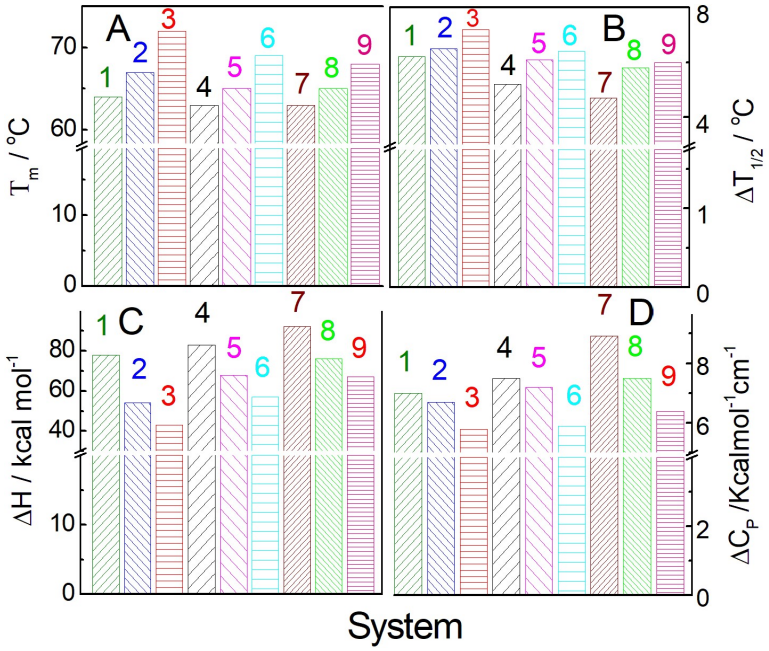

Figure 18. Variations of chain melting temperature (T_m, A), width at half peak height ($\Delta T_{1/2}$, B), enthalpy change (ΔH, C) and corresponding heat capacities (ΔC_p, D) of different metallosurfactants at 298K. System: 1, $[(C_{12}Mal)_2Cd_2]$; 2, $[(C_{12}Mal)_2Ca_2]$; 3, $[(C_{12}Mal)_2Mn_2]$; 4, $[(C_{12}Asp)_2Cd_2]$; 5, $[(C_{12}Asp)_2Ca_2]$; 6,$[(C_{12}Mal)_2Mn_2]$; 7, $[(C_{12}Glu)_2Cd_2]$; 8, $[(C_{12}Glu)_2Ca_2]$ and 9, $[(C_{12}Glu)_2Mn_2]$.

With decreasing the size of the bivalent metal ($Cd^{2+} > Ca^{2+} > Mn^{2+}$), T_m values are increased. Bivalent metals electrostatically interacted with $(C_{12}AAS)Na_2$ and relatively sharp peak appeared that indicate stronger head group packing. Lowering of T_m is due to size enhancement as well as increased specific surface area.[274] The T_m values of manganese metallosurfactants are higher than Ca and Cd because widening of the peaks that designated multi-crystallinity and heterogeneity. Two dicarboxylate groups of $(C_{12}AAS)Na_2$ get progressively separated by extra methylene groups whereby increasing the distance between two carboxylate anion from $C_{12}MalNa_2$ to $C_{12}GluNa_2$ via $C_{12}AspNa_2$. The $\Delta T_{1/2}$ values of manganese metallosurfactants are lower than Ca and Cd due to the tilting of the two hydrophobic parts of $(C_{12}AAS)Na_2$. Electrostatic interaction between $(C_{12}AAS)Na_2$ with M^{2+} results increasing in the crystal imperfection, led to increased $\Delta T_{1/2}$ values. With increasing the size of the bivalent metal, $\Delta T_{1/2}$ values gradually decreased that indicates better packing of the hydrophilic moieties over layer like oppositely charged head groups. With decreasing the size of bivalent metals, ΔH value gradually increases that

indicates endothermic peak due to the organization of bivalent metal over layer around the crystal. The ΔH values are found to be higher due to the higher hydrophobic interaction between bivalent metal and $(C_{12}AAS)Na_2$. $(C_{12}AAS)Na_2$ are weakly interacted with Ca^{2+} and Cd^{2+} than Mn^{2+} that indicate lower T_m value. Lower values of ΔH and ΔCp for the metallosurfactants were due to the increased multicrystallinity.

3.1.5. Thermo gravimetric analysis (TGA) studies. Phase transition and associated weight loss of metallosurfactants were performed by TGA studies.[269-271] Results on the thermogravimetric analysis of the metallosurfactants have been summarized in Figure 16 (panel B) and data was shown Table 1.

Table 1. Results on the thermogravimetric analysis of synthesized metallosufactants $[(C_{12}AAS)_2M_2]$ systems.

System	Name of metallosurfactants	Temperature range	% wt. remaining
$[(C_{12}Mal)_2Cd_2]$	dicadmium (didodecylamino malonate)	80-105	89
		105-186	79
		247-310	68
$[(C_{12}Asp)_2Cd_2]$	dicadmium (didodecylamino aspartate)	86-125	93
		260-310	77
		310-345	51
$[(C_{12}Glu)_2Cd_2]$	dicadmium (didodecylamino glutamate)	73-143	90
		272-316	78
		310-344	55
$[(C_{12}Mal)_2Ca_2]$	dicalcium (didodecylamino malonate)	51-120	94
		113-158	81
		185-263	77
$[(C_{12}Asp)_2Ca_2]$	dicalcium (didodecylamino aspartate)	43-102	87
		232-259	67
		263-320	48
$[(C_{12}Glu)_2Ca_2]$	dicalcium (didodecylamino glutamate)	93-143	80
		268-382	52
		310-420	18
$[(C_{12}Mal)_2Mn_2]$	dimanganese (didodecylamino malonate)	43-109	81
		119-288	63
		290-360	36
$[(C_{12}Asp)_2Mn_2]$	dimanganese (didodecylamino aspartate)	85-130	87
		168-274	68
		289-385	31
$[(C_{12}Glu)_2Mn_2]$	dimanganese (didodecylamino glutamate)	58-113	82
		188-289	64
		296-390	24

3.2. Interfacial studies on the metallosurfactants.

3.2.1. Surface pressure (π) - area (A) isotherm. At different metallosurfactant / SPC ratio, in combination with 30 mole% cholesterol (to mimic the eukaryotic cell membrane) surface pressures (π) - area (A) isotherms were recorded at air-water interface (Figure 19-20).

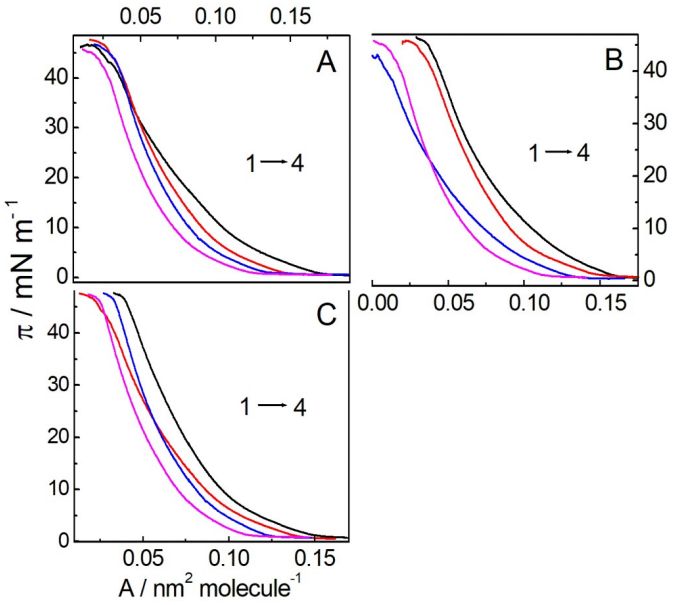

Figure 19. Surface pressure (π) - area (A) isotherms of $(C_{12}AAS)_2M_2$+SPC mixed monolayers at air-water interface at 298K. Systems: panel A, $(C_{12}Glu)_2Mn_2$+SPC; $(C_{12}Glu)_2Ca_2$+SPC and C, $(C_{12}Glu)_2Cd_2$+SPC. Mole fractions of $(C_{12}AAS)_2M_2$: 1, 0.8; 2, 0.6; 3, 0.4 and 4, 0.2. 30 mole% cholesterol was used in each case.

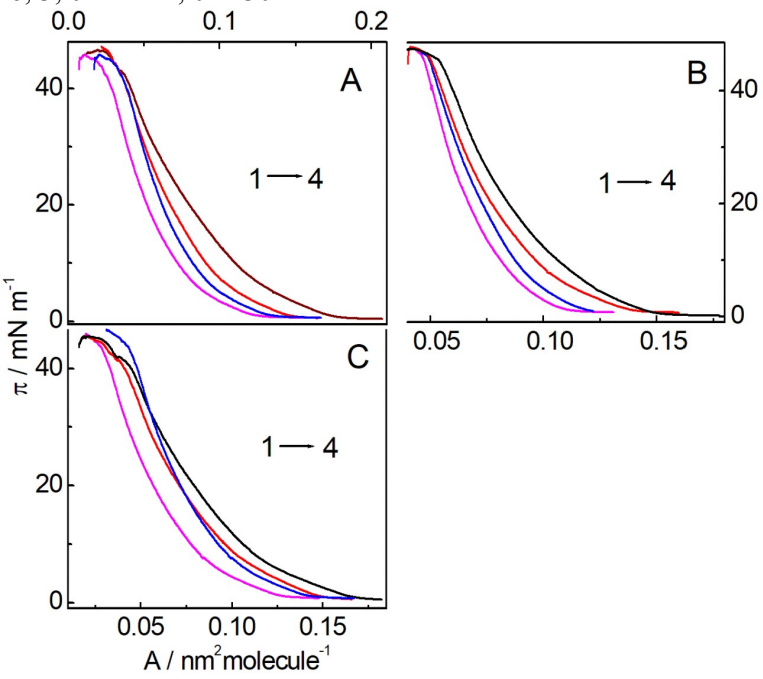

Figure 20. Surface pressure (π) - area (A) isotherms of $[(C_{12}AAS)_2M_2]$+SPC mixed monolayers. Systems: panel A, $[(C_{12}Asp)_2Mn_2]$+SPC; B, $[(C_{12}Asp)_2Ca_2]$+SPC and C, $[(C_{12}Asp)_2Cd_2]$+SPC at air-water interface at 298K. Mole-fraction of $[(C_{12}AAS)_2M_2]$, $\alpha_{(C_{12}AAS)_2M_2}$: 1, 0.0; 2, 0.2; 3, 0.4; 4, 0.5; 5, 0.6; 6, 0.8 and 7, 1.0. 30 mole% cholesterol was used each cases.

Different physicochemical parameter, *viz.,* lift-off area (A_0), minimum molecular area (A_{min}), collapse pressure (π_c) molecular organization, subsequent interaction, thermodynamics of the interaction processes between the components and film compressibility were evaluated from the π - A isotherms.[123] π_c, A_0 and A_{min} values of different $(C_{12}AAS)_2M_2$ profiles are shown in Figure 21. Hydrophobic interaction between the two long chain hydrocarbons of $C_{12}GluNa_2$ are higher than $C_{12}AspNa_2$ and $C_{12}MalNa_2$ henceforth A_0 and A_{min} values of $C_{12}GluNa_2$ is higher than $C_{12}MalNa_2$ via $C_{12}AspNa_2$. Smaller Mn^{2+} ion has higher charge density; hence it interacts with the carboxylate ion more strongly than larger size transition metals like Cd^{2+} and Ca^{2+}. For higher charge density on Mn^{2+}, these metallosurfactants did not get sufficient opportunity for reorganization of molecular packing whereby π_c values got upshifted. Smaller size Mn^{2+} electrostatically interact strongly with $(C_{12}AAS)Na_2$, forms expanded mixed monolayer henceforth A_0 and A_{min} values are higher than Cd^{2+} and Ca^{2+} that follows the sequence: $(C_{12}Glu)_2Mn_2$ > $(C_{12}Asp)_2Mn_2$ > $(C_{12}Mal)_2Mn_2$ > $(C_{12}Glu)_2Ca_2$ > $(C_{12}Asp)_2Ca_2$ > $(C_{12}Mal)_2Ca_2$ > $(C_{12}Glu)_2Cd_2$ > $(C_{12}Asp)_2Cd_2$ > $(C_{12}Mal)_2Cd_2$. Cholesterol shows condensation effect of mixed monolayer. A_0 of SPC in presence of 30 mole% cholesterol appeared at 1.1 nm^2 $molecule^{-1}$.[154]

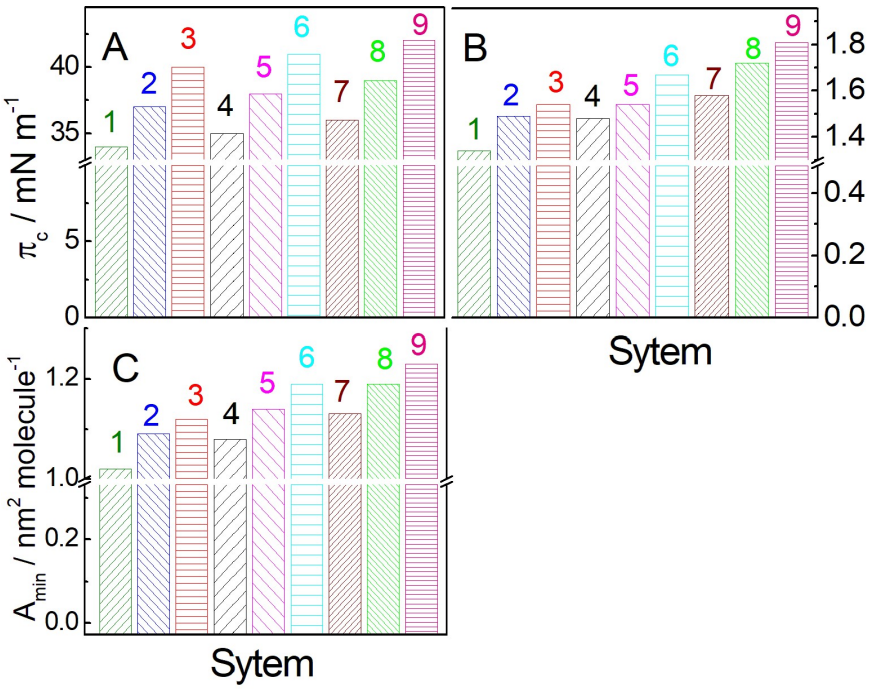

Figure 21. Variations of collapse pressure (π_c, A), lift-off area (A_0, B) and minimum molecular area (A_{min}, C) of different metallosurfactants at 298K. System: 1, $[(C_{12}Mal)_2Cd_2]$; 2,$[(C_{12}Mal)_2Ca_2]$; 3, $[(C_{12}Mal)_2Mn_2]$; 4, $[(C_{12}Asp)_2Cd_2]$; 5, $[(C_{12}Asp)_2Ca_2]$; 6, $[(C_{12}Mal)_2Mn_2]$; 7, $[(C_{12}Glu)_2Cd_2]$; 8, $[(C_{12}Glu)_2Ca_2]$ and 9, $[(C_{12}Glu)_2Mn_2]$.

In case of $(C_{12}AAS)_2M_2$+SPC mixed monolayers with increasing mole fraction of $\alpha_{(C_{12}AAS)_2M_2}$, A_0 values gradually increase, indicating renovation of molecular packing and expanded monolayer at air-water interface. With increasing $\alpha_{(C_{12}AAS)_2M_2}$, π_c values do not change significantly because of reorganization of molecular packing. With increasing $\alpha_{(C_{12}AAS)_2M_2}$, A_{min} values increased due to the loss of the molecule from the surface monolayer and sub phase. Although formation of vesicle, van der Waals interaction between $(C_{12}AAS)_2M_2$ and SPC which overcome the columbic force of attraction by the choline head group of SPC.

Ideal value of molecular area (A_{id}) of mixed monolayer was calculated by additivity rule:[303]

$$A_{id} = x_1A_1 + x_2A_2 \quad (5)$$

where average theoretical area per molecule is A_{id}, x_1 and x_2 being the mole fraction of component-1 (SPC + 30 mole% cholesterol) and component-2 $(C_{12}AAS)_2M_2$+ 30 mole% cholesterol), respectively. A_1 corresponds to the molecular area of component 1 and A_2 corresponds to the same for the component 2. Excess molecular area (A_{ex}), a parameter that corresponds to the deviation of the experimental value from the theoretically calculated value, can be calculated as:[295]

$$A_{ex} = A_{12} - A_{id} \quad (6)$$

where A_{12} is the experimental area per molecule of mixed monolayer system.

Variations of A_{ex} with $\alpha_{(C_{12}AAS)_2M_2}$ are shown in Figure 22. At 20 and 60 mole% $(C_{12}AAS)_2M_2$ monolayer displays positive deviations. Chain mismatching of $(C_{12}AAS)_2M_2$+SPC mixed monolayers exhibit positive deviation from ideality. At 40, 50 and 80 mole% of $(C_{12}AAS)_2M_2$ associative interactions are recorded which are due to the hydrophobic interaction between $(C_{12}AAS)_2M_2$ and SPC. Negative deviations from the ideal values implies associative interaction and vice versa. Variation of A_{ex}/A_{id} with $\alpha_{(C_{12}AAS)_2M_2}$, has shown in Figure 22.

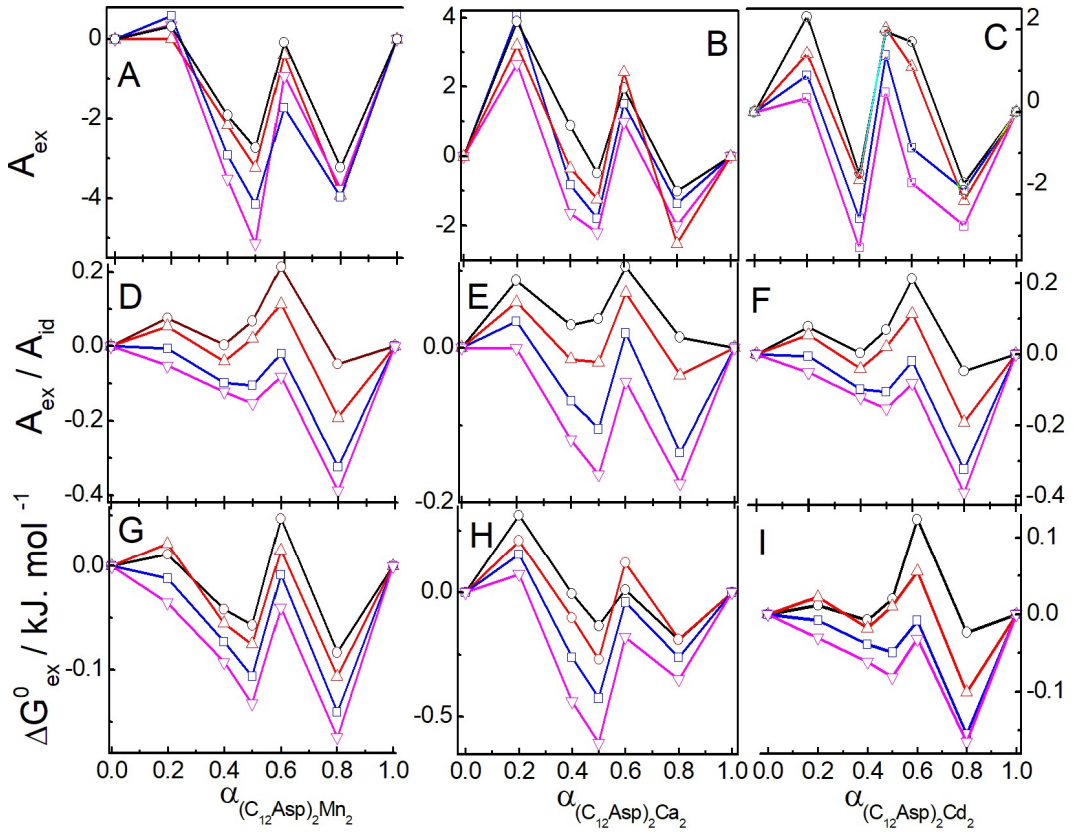

Figure 22. Variations of (A_{ex}, A, B, C), (A_{ex}/A_{id}, D, E, F) and (ΔG_{ex}, G, H, I) for the [$(C_{12}Asp)_2Mn_2$]+SPC, [$(C_{12}Asp)_2Ca_2$]+SPC and [$(C_{12}Asp)_2Cd_2$]+SPC mixed monolayer in the presence of 30 mole% cholesterol with different mole-fraction of [$(C_{12}Asp)_2Mn_2$], [$(C_{12}Asp)_2Ca_2$] and [$(C_{12}Asp)_2Cd_2$] at different surface pressure. Surface pressures (mNm^{-1}): ○, 5; Δ, 10; □; 20 and ∇, 30. Temperature: 298K.

Change in Gibbs excess free energy (ΔG^0_{ex}) and free energy of mixing (ΔG^0_{mix}) were calculated by suitably processing the π - A isotherms using the following equation:[154]

$$\Delta G^0_{ex} = \int_0^{\pi} (A_{12} - A_{id}) d\pi \quad (7)$$

$$\Delta G^0_{ideal} = RT\,[(x_1\, ln x_1 + x_2\, ln x_2)] \quad (8)$$

$$\Delta G^0_{mix} = \Delta G^0_{ex} + \Delta G^0_{ideal} \quad (9)$$

ΔG^0_{ex} *vs.* profile for the $(C_{12}Glu)_2Mn_2$+SPC system has been shown Figure 22. This results clearly indicate that non-ideal mixing between $(C_{12}AAS)_2M_2$ and SPC is prevalent for all the combinations. In case of $(C_{12}AAS)_2M_2$+SPC mixture at 40, 50 and 80 mole% of $(C_{12}Glu)_2Mn_2$ negative ΔG^0_{ex} are due to favorable arrangement of mixed monolayer and spontaneous micellization. At 20 and 60 mole% of $(C_{12}AAS)_2M_2$ exhibit lower ΔG^0_{ex} value, that indicate non-spontaneous mixing process due to the chain mismatching. In case of $(C_{12}AAS)_2M_2$+SPC mixture at 50 mole% of $(C_{12}AAS)_2M_2$ negative ΔG^0_{mix} is

observed that indicate strong hydrophobic interaction between the two long chain hydrocarbons of $(C_{12}AAS)_2M_2$ and SPC. At 20 and 80 mole% of $(C_{12}AAS)_2M_2$ positive ΔG^0_{mix} values are due to two anionic carboxylate parts of $(C_{12}AAS)Na_2$ that are dissociated in the presence of the negatively charged phosphate ion of the choline group and associative interaction between the M^{2+} and phosphate group of SPC.

Monomolecular film compressibility (C_s) is the resistance of a monolayer against compression.[303] Reciprocal of compressibility (C_s^{-1}) is known as film compression modulus. Compression modulus values are calculated from following equation for different mixed composition.[154]

$$C_s^{-1} = -A\left(\frac{\delta\pi}{\delta A}\right) \tag{10}$$

Representative variations of film compressibility with surface pressure are shown in Figure 23.

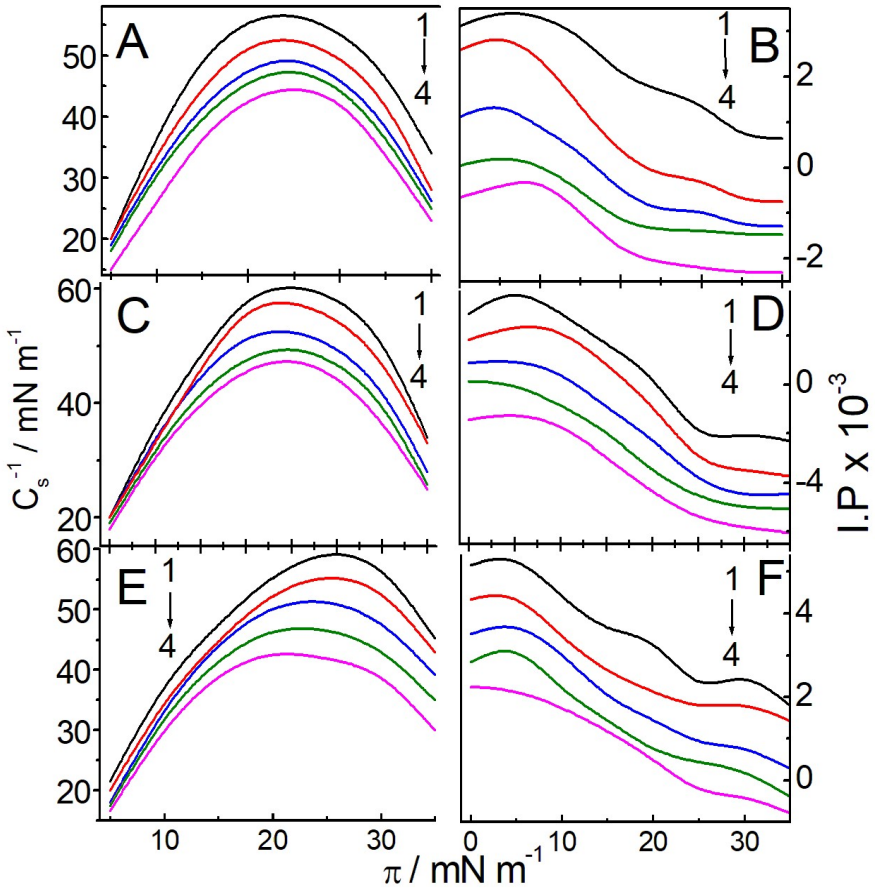

Figure 23. Variations of compressibility modulii (C_s^{-1}, A, C, E) and interaction parameter (*I.P.*, B, D, E) with the surface pressure of $[(C_{12}Asp)_2Mn_2]$+SPC, $[(C_{12}Asp)_2Ca_2]$+SPC and $[(C_{12}Asp)_2Cd_2]$+SPC mixed monomolecular films with 30 mole% cholesterol. Mole% of $[(C_{12}AAS)_2M_2]$, $\alpha_{C_{12}AAS_2M_2}$: 1, 0.2; 2, 0.4; 3, 0.5 ; 4, 0.6 and 5, 0.8. Temperature: 298K.

With decreasing $\alpha_{(C_{12}AAS)_2M_2}$, C_s^{-1} values gradually increase and vary from 10 to 50 mNm^{-1} in the liquid expanded phase.[123] At 20 mNm^{-1} pressure maximum C_s^{-1} values are observed that gradually decrease indicating the formation of viscous monolayer. C_s^{-1} values gradually decreased with increasing $\alpha_{(C_{12}Glu)_2Mn_2}$, indicating monolayers are more compressible than saturated analogues. $(C_{12}AAS)_2M_2$ and acyl chain of SPC are saturated and the monomolecular films are less compressible.

Interaction parameter (*I.P.*) of mixed monolayer was derived using the following equation:[154]

$$w = \frac{\Delta G_{ex}^0}{X_1 X_2} \tag{11}$$

$$I.P. = \frac{w}{RT} \tag{12}$$

I.P. is the function of surface pressure (π), *I.P. vs* π at different composition of $(C_{12}AAS)_2M_2$+SPC mixed monolayer profile is shown in Figure 23. With decreasing $\alpha_{(C_{12}AAS)_2M_2}$, *I.P.* values linearly increase up to 20 mNm^{-1} then passing through constant values, that indicates formation of viscous and rigid monolayer at air-water interface. With decreasing $\alpha_{(C_{12}Glu)_2Mn_2}$, *I.P.* values become higher because acyl chain of SPC turn hold the saturated hydrocarbon chain of $(C_{12}AAS)_2M_2$ due to the dominant of SPC in the mixed monolayer. *I.P.* results clearly indicate that rigid and spontaneous mixed monolayer are formed the results are well correlated with the ΔG_{ex}^0 and surface elasticity studies.

3.2.2. Dilatational surface rheology studies. Measurements of the dynamic surface elasticity were provided for mixtures of metallosurfactants and SPC at different mole% Figure 24 (panel A). The dynamic surface elasticity abruptly increases up to 20 mN/m for all the mixtures when π starts to increase from zero to about 1.5 mN/m, that indicates the formation of relatively rigid spread monolayers. Further increasing of π under compression of monolayer surface elasticity values gradual increased. The dynamic surface elasticity slightly increases with decrease of $\alpha_{(C_{12}AAS)_2M_2}$, however, it is more important that the decrease of $\alpha_{(C_{12}AAS)_2M_2}$, leads to an increase of the surface pressure range, where one can measure the dynamic surface elasticity. At high $\alpha_{(C_{12}AAS)_2M_2}$, and high π the monolayer is unstable and measurements of the dynamic surface elasticity become impossible. Probably, molecules of metallosurfactants are

displaced from the interface and start to dissolve in the subphase. This effect is confirmed by measurements of compression isotherms at different rates of deformation.

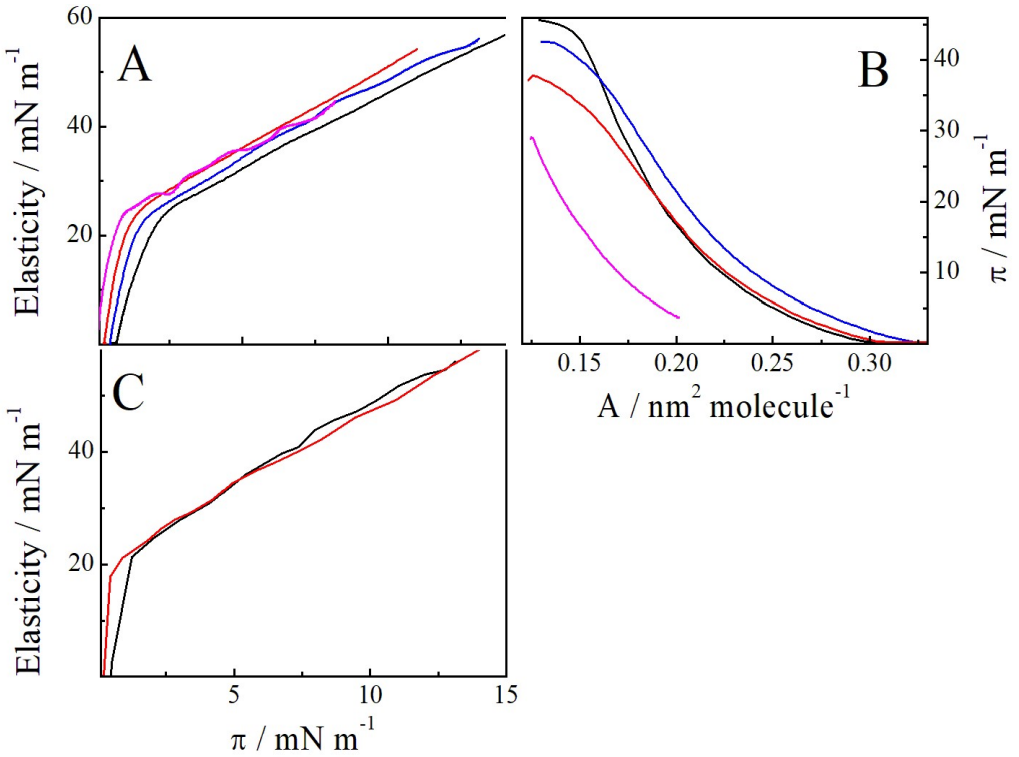

Figure 24. Panel A: surface elasticity *vs.* surface pressure dependencies for monomolecular films of $(C_{12}Mal)_2Ca_2$+SPC at Mal mole fractions: 0.8 (magenta line); 0.6 (red line); 0.5 (blue line); 0.2 (black line). Panel B: surface pressure-area dependencies for monomolecular films of $(C_{12}Mal)_2Ca_2$+SPC at Mal mole fraction 0.5 and different rates of surface compression: 2 (magenta line); 5 (red line); 10 (blue line); 50 mm/min (black line). Panel C: surface elasticity *vs.* surface pressure dependencies isotherms for monomolecular films of $(C_{12}Mal)_2Ca_2$+SPC (red line) and $(C_{12}Mal)_2Cd_2$+SPC (black line). $(C_{12}AAS)Na_2$ mole fraction is 0.5.

Figure 24 (panel B) shows that the isotherms depend on the rate of surface compression. The surface pressures corresponding to the same surface concentrations increase with the increase of the compression rate. Moreover, the maximal surface pressure, the collapse pressure, also increases with the increase of compression rate. It should be noted that substitution of Ca^{2+} by Cd^{2+} in metallosurfactants results in the expanding of surface pressure range, which is accessible for measurement of the surface elasticity Figure 24 (panel C). This means that mixed monolayer of metallosurfactants and SPC are more stable in case of the substitution by Cd^{2+}.

3.2.3. BAM images of mixed monomolecular films. Investigation of mesoscopic structure of mixed monolayers of metallosurfactant and SPC was provided by BAM. Figure 25 presents the results of BAM images for mixed monolayers with 40 mole% of $(C_{12}Glu)_2Ca_2$ at different surface pressures. All the images demonstrate homogeneous structure of the surface layer confirming the miscibility of the components. The brightness of images increases with increasing of the surface pressure due to the increase of the surface concentration and the formation of a more condensed structure.

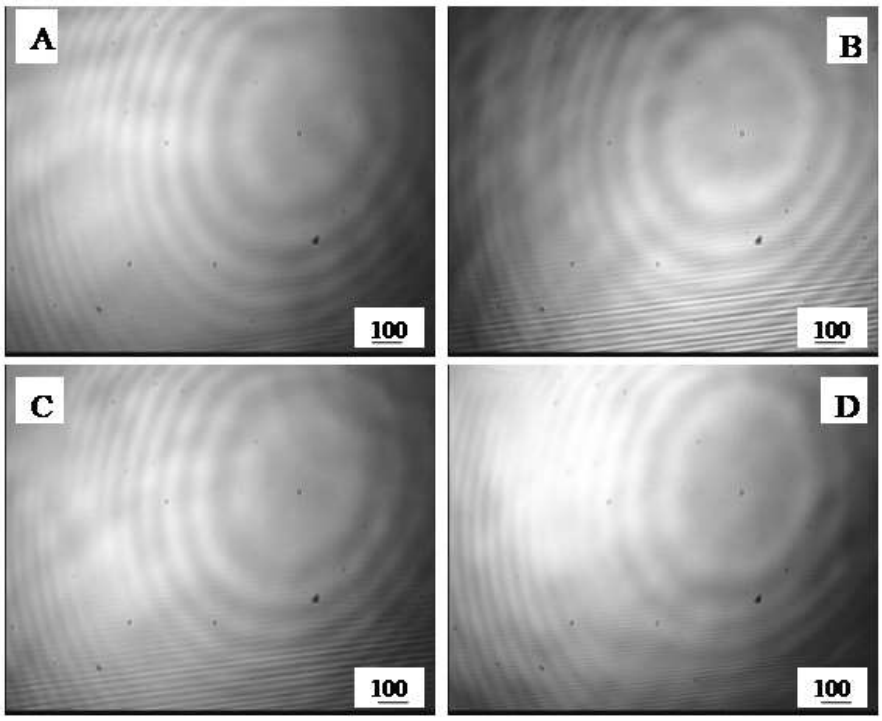

Figure 25. BAM images of $(C_{12}Glu)_2Ca_2$+SPC mixed monolayers, $(C_{12}Glu)_2Ca_2$/SPC (0.2:0.3 M/M). Surface pressure π (mN/m): = A, 0; B, 10; C, 20 and D, 30. White bar represent 100µm. Temperature: 298K.

Lamellar structure, and mixed monolayer results confirmed that pseudo double tailed bivalent metallosurfactants $[(C_{12}AAS)_2M_2]$ have been formed. Molecular modeling and diffusion NMR had also supported formation of dimmers. However, discussions about this result are beyond the scope of this article and will be published in our future articles. Structures of the synthesized metallosurfactants are shown in Scheme 1.

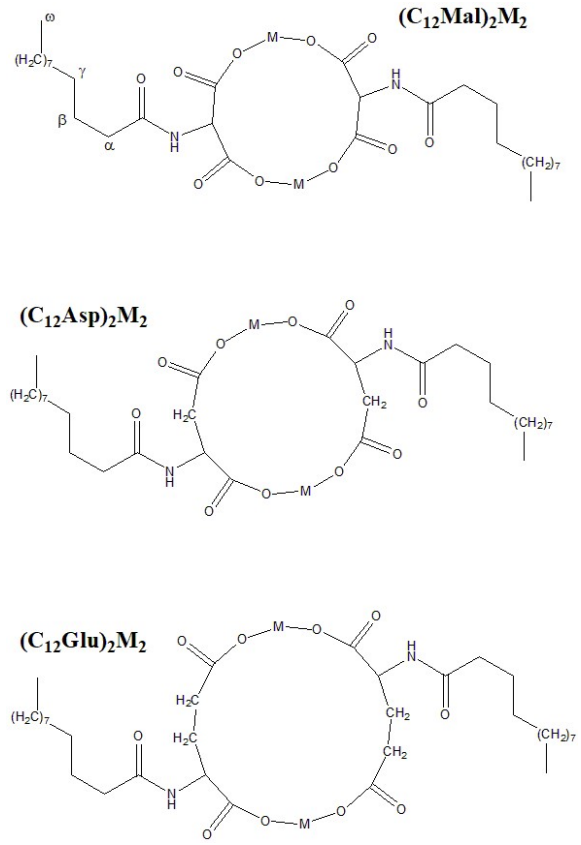

Scheme 1: Dimeric structures of metallosurfactants. M = Cd, Ca, Mn. Names of individual compounds can be found in Table 1.

3.2.4. Dynamic light scattering (DLS) studies. Hydrodynamic diameter (d_h) and zeta potential (*Z.P.*) values revealed the stability and bio distribution of vesicles. Polydispersity index is another parameter describing the size distribution. Stability of the vesicles for different compositions [$(C_{12}AAS)_2M_2$/SPC ratio] in combination with 30 mole% cholesterol were investigated by DLS studies. Size *vs.* time profile was shown in Figure 26 (panel A) as well as results were shown in Table 2.

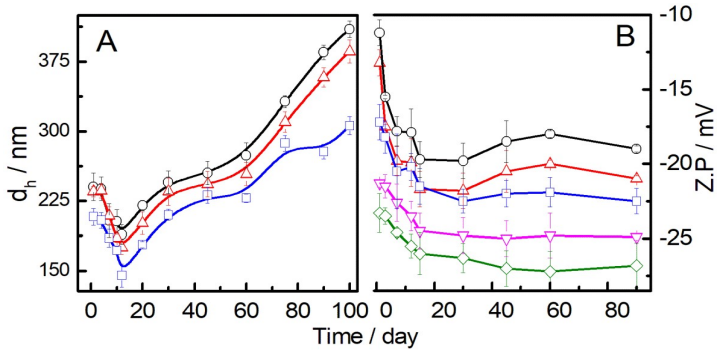

Figure 26. Variations in the hydrodynamic diameter (d_h, A) and zeta potential (*Z.P*, B) for $(C_{12}Glu)_2$ Ca_2+SPC (in the presence of 30 mole% cholesterol) with time. System: mole-fractions of $(C_{12}Glu)_2Ca_2$, $\alpha_{(C_{12}Glu)_2Ca_2}$: □, 0.2; ○, 0.4; △, 50; ∇, 60 and ◊; 80. Temperature: 298K.

Table 2. Hydrodynamic diameter (d_h), zeta potential (*Z.P.*) and polydispersity index (*PDI*) values of different vesicle formulation systems at 298K. This data was taken on the day 45 of the sample preparation.

system	d_h/ nm	*Zeta*/ mV	*PDI*
$\alpha_{C_{12}AAS_2M_2}$	**$[(C_{12}Mal)_2Mn_2]$+SPC**		
0.8	231	-2.50	0.31
0.6	243	-6.00	0.41
0.5	255	-8.00	0.42
0.4	256	-9.00	0.52
0.2	275	-10.0	0.72
0.0	220	-18.5	0.28
	$[(C_{12}Asp)_2Mn_2]$+SPC		
0.8	214	-6.50	0.27
0.6	245	-10.0	0.46
0.5	247	-10.4	0.47
0.4	298	-12.0	0.52
0.2	302	-16.8	0.61
	$[(C_{12}Glu)_2Mn_2]$+SPC		
0.8	225	-4.50	0.28
0.6	245	-6.00	0.45
0.5	259	-9.00	0.46
0.4	284	-10.0	0.56
0.2	287	-13.0	0.58
	$[(C_{12}Mal)_2Ca_2]$+SPC		
0.8	231	-2.50	0.30
0.6	243	-6.00	0.42
0.5	255	-8.00	0.52
0.4	256	-9.00	0.54
0.2	275	-10.0	0.58
	$[(C_{12}Asp)_2Ca_2]$+SPC		
0.8	224	-6.50	0.46
0.6	245	-9.20	0.48
0.5	278	-11.0	0.49
0.4	289	-15.9	0.54
0.2	298	-16.8	0.56
	$[(C_{12}Glu)_2Ca_2]$+SPC		
0.8	256	-7.50	0.24
0.6	278	-9.00	0.25
0.5	289	-11.9	0.45
0.4	298	-13.2	0.54
0.2	298	-15.5	0.56
	$[(C_{12}Glu)_2Cd_2]$+SPC		
0.8	260	-7.50	0.24
0.6	272	-10.0	0.32
0.5	282	-13.9	0.45
0.4	292	-15.2	0.52
0.2	320	-17.5	0.54

Most of the hybrid vesicles were fairly stable up to 100 days. Vesicles experienced size contraction during first 10-15 days, after which vesicle sizes gradually increased. During first 10-15 days time-period, the forcefully dispersed lipids and metallosurfactants in vesicles undergo flipping and reorganization, that results size contraction. Subsequent size growths in vesicles are considered to be due to vesicle aggregation. With decreasing $\alpha_{(C_{12}AAS)_2M_2}$, size of the vesicles gradually increased due to synergistic interaction between $(C_{12}AAS)_2M_2$ and SPC; besides larger number of water molecule that hydrate the vesicle palisade layer, are considered to stabilize the vesicle.

PDI value of a colloidal dispersion corresponds to its heterogeneity in size distribution. *PDI* values of vesicles were in the range 0.2 to 0.7, results homogeneous dispersion of the lipid phase during vesicles preparation. With decreasing $\alpha_{(C_{12}AAS)_2M_2}$, *PDI* values of mixed liposome were significantly increased, this variation indicates that change the surface homogeneity of vesicles as well as formation of homogeneous colloidal particles.

It is known that colloidal particles are charged which impart its kinetic stability. Surface charge and stability of vesicles can suitably be evaluated by measuring its zeta potential (*Z.P.*). *Z.P.* values of vesicle of different compositions were monitored up to 45 days from the day of sample preparation; representative results are shown in Figure 26 (panel B). Zeta potential values varied unsystematically up to 15 days after which this value did not change significantly due to the instability of vesicle. After 20 days *Z.P.* values are constant because after ionization colloidal particles did not associated or dissociated only some M^{2+} are dissociated henceforth *Z.P.* did not change significantly. Negative zeta potential of mixed liposome indicates that electrostatic stabilization along with lipidic dispersion as well as prevents the formation of aggregates. Zeta potential value of SPC was -19.7 mV. With increasing $\alpha_{(C_{12}AAS)_2M_2}$, *Z.P.* values were moved towards negative direction. With increasing $\alpha_{(C_{12}AAS)_2M_2}$, negative *Z.P.* values were observed due to the dissociation of $(C_{12}AAS)_2M_2$ leaves dianionic carboxylic $(C_{12}AAS)Na_2$ in the bilayer.

3.2.5. Transmission electron microscopy (TEM) studies. Size, shape, surface morphology and bilayer thickness of vesicles were studied by TEM.[155] Representative TEM images of vesicle with 30 mole% cholesterol were shown in the Figure 27. Vesicles exhibited spherical morphology where the sizes were in the range of 100-500 nm. Results are found to be comparable with the DSL studies, although smaller in dimensions which are considered due to the differences in methodologies.

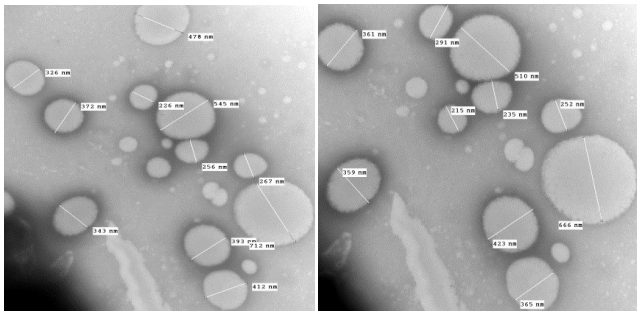

Figure 27. Representative TEM images of $(C_{12}Glu)_2Ca_2$+SPC mixed vesicle $(C_{12}Glu)_2Ca_2$:SPC, 6:4 (M/M). Temperature: 298K.

3.2.6. Cytotoxicity studies. Cytotoxicity is the biological evaluation and screening test that use tissue cells *in vitro* to observe the cell growth.[304] Vesicles comprising metallosurfactants, SPC and cholesterol were mostly non-toxic,[253] as summarized in Figure 28.

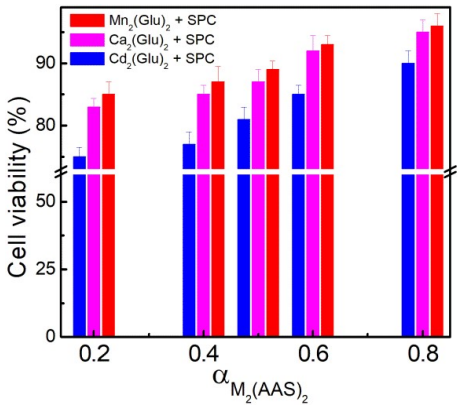

Figure 28. Variation of human blood lymphocyte cell viability (%) with $\alpha_{C_{12}AAS_2M_2}$ of $[(C_{12}AAS)_2M_2]$+SPC mixed vesicles in the presence of 30 mole% of cholesterol. Concentration of $[(C_{12}AAS)_2M_2]$+SPC: 0.1 mM.

At 20 mole% of $(C_{12}AAS)_2M_2$, vesicles show more than 65% cells to be viable and 40 mole% of $(C_{12}AAS)_2M_2$ shows low cytotoxicity. At 80 mole% of $(C_{12}AAS)_2M_2$, liposomes are able to cease bacterial growth and at the same concentration cell viability of the lymphocytes was > 93%. $(C_{12}AAS)_2M_2$+SPC mixed liposomes exhibited higher MIC and toxicity that indicates less therapeutic value.[251] In the present study, vesicles show low cytotoxicity towards human peripheral lymphocytes.

Vesicles were displayed lower cytotoxicity which indicates its higher therapeutic application and easily applicable for drug delivery system. The obtained results showed that $(C_{12}AAS)_2M_2$+SPC mixed liposome are nontoxic.[305] Thus, the dosage of $(C_{12}AAS)_2M_2$+SPC mixed liposome at > 60 mole% of $(C_{12}AAS)_2M_2$ were found to be hemocompatible.

4. Conclusions. Formations of coacervates of $(C_{12}AAS)_2M_2$ were ensured with NMR and FTIR as well as layered structures were supported by XRD studies. Thermal phase transition, weight loss and liquid crystalline nature are confirmed from TGA and DSC measurements. Monomolecular films of the metallosurfactants in combination with soy phosphatidylcholine (SPC) and cholesterol were investigated using a Langmuir surface balance. With increasing $\alpha_{(C_{12}AAS)_2M_2}$, mean molecular area values gradually increased, indicating reorganization of molecular packing and formation of expanded monolayer at air-water interface, whereby interfacial adsorption and non-spontaneous mixing behaviors were confirmed with negative ΔG_{ex}^{0}. Dynamic surface elasticity, values of mixed monolayers, initially increased in the surface pressure range from 0 to 1.5 mN/m, after which the slope of surface elasticity *vs.* surface pressure profiles gradually decreased indicating formation of rigid monolayers. BAM images demonstrated qualitative information of homogeneous and condensed structure of mixed monolayer, as well as suggested two dimensional phase transition upon compression of the monolayer. Metallosurfactants in combination with SPC and cholesterol were formed stable hybrid vesicles. Hydrodynamic diameter, zeta potential and polydispersity index values of vesicles were measured by dynamic light scattering studies, monitored as function of time to check its stability; particles were found to be stable up to 100 days. Hydrodynamic diameter and negative zeta potential of the vesicles gradually increased with increasing $\alpha_{(C_{12}AAS)_2M_2}$, due to the hydrophobic interaction between oppositely charged surfactants. TEM images demonstrated formation of spherical vesicles results correlated with DLS studies. Cytotoxicity studies indicate liposomes are nontoxic. It is clear that $(C_{12}AAS)_2M_2$+SPC mixed liposome used as potential drug carrier. *In vitro* cytotoxicity study revealed that hybrid vesicles could act as promising vehicles for drugs with controlled and sustained release.